Title

Incorporating Enzymatic Nanoparticles with the Lateral-Flow Immunoassay for Improved Diagnostic Capabilities

Author

Ryan, Milo James Worley

Publication Date

2022

Peer reviewed|Thesis/dissertation

UNIVERSITY OF CALIFORNIA

Los Angeles

Incorporating Enzymatic Nanoparticles with the Lateral-Flow Immunoassay for Improved Diagnostic Capabilities

A thesis submitted in partial satisfaction of the

requirements for the degree Master of Science

in Bioengineering

by

Milo James Worley Ryan

2022

ABSTRACT OF THE THESIS

Incorporating Enzymatic Nanoparticles with the Lateral-Flow

Immunoassay for Improved Diagnostic Capabilities

by

Milo James Worley Ryan
Master of Science in Bioengineering
University of California, Los Angeles, 2022
Professor Daniel T. Kamei, Chair

The COVID-19 pandemic has underscored the global need for rapid, widespread testing to avoid the spread of infectious diseases via early detection. The benefits of early diagnosis are not only limited to infectious diseases, as early detection of both communicable and noncommunicable diseases are associated with positive health outcomes.

While current gold standard diagnostics return accurate results, they require expensive lab equipment and trained personnel making them difficult to use in resource-limited settings where the burden of disease is greatest. To achieve rapid, widespread diagnosis in resource-limited settings, there is a need to develop low-cost diagnostic devices. One such device is the lateral-flow immunoassay (LFA). The LFA is suitable for point-of-care diagnosis in resource-limited settings,

but it suffers from limited sensitivity and lack of quantitative results. The focus of this thesis is to develop techniques which address the limitations of the LFA.

In Chapter 2, we focus on increasing the sensitivity of the LFA to detect the SARS-CoV-2 nucleocapsid protein (N-protein). To do so, we developed a 3D printed casing that incorporates the LFA, dehydrated signal enhancements reagents, and a buffer reservoir. After applying a sample, the user simply needs to press a single button to detect the SARS-CoV-2 N-protein at concentrations as low as 0.1 ng/mL in just 40 minutes.

In Chapter 3, we develop a semi-quantitative assay using the LFA to detect digoxin in human serum. Digoxin is a cardiac glycoside used to treat atrial fibrillation (AF) and has a narrow therapeutic range, above which it can be toxic. Therefore, it requires continual monitoring of serum concentrations to ensure safe and effective administration. To achieve the necessary quantitative capabilities to measure digoxin concentration, we integrated the conventional LFA with the anisotropic etching of gold nanorods (GNRs). This integrated setup achieves a multicolor, semi-quantitative assay that can be interpreted by the naked eye to determine digoxin concentrations in serum within the relevant range of 0.5 to 3 ng/mL.

The thesis of Milo James Worley Ryan is approved.

Benjamin M. Wu

Timothy J. Deming

Daniel T. Kamei, Committee Chair

University of California, Los Angeles

2022

This work is dedicated to my family who have unconditionally supported me.

TABLE OF CONTENTS

LIST OF FIGURES

ACKNOWLEDGMENTS

This work could not have been completed without the guidance and support of many people. Firstly, I would like to thank my mentor Dr. Daniel T. Kamei. His continual input truly helped me develop into the researcher that I am today. With his help I was able to not only develop my research and critical thinking skills, but also my work ethic and my self-confidence as he helped me realize just what I was capable of. I truly cannot imagine where I would be without his support.

Next, I would like to thank Dr. Daniel W. Bradbury who was my graduate student mentor during my undergraduate years in the lab. When I first joined the team, he helped guide me through experiments as I grew as a researcher. Later on, he allowed me to flourish and took a step back to offer guidance whenever I needed it. My goal when I joined the lab was to be able to emulate the way that he approached problems and systematically worked through his trials. However, outside of research I am also glad I can call him a friend. He introduced me to the vast world of coffee, that has developed into a staple in my everyday life. He was a major part not only in my growth as a researcher, but also the projects presented in this thesis.

Next, I would like to thank Jasmine Trinh. I have worked side-by-side with Jasmine all throughout my time in lab and she was an integral part of the projects presented in this thesis. She is a brilliant researcher and being able to work with her has been an absolute pleasure and helped me become an even better researcher. She is also an incredible friend who has been there for me on numerous occasions. During my time in the graduate program, I have also been incredibly lucky to work with Frances Nicklen, Jerry Lu, Paula Pandolfi, Alexia Diaz, Cecilia Zhang and Salil Patel.

Frances Nicklen and Jerry Lu were part of the research project presented in Chapter 2. While I didn't get the chance to work with all of them on a research project, being surrounded by such a great group of people has been a blessing. Furthermore, I am grateful to Cassandra Cantu, Kyle Chen and Adel Battikha for their work on the projects presented in this thesis.

Finally, I would like to thank my family and friends who have truly supported me throughout my entire life. Without all of you I would not be the person that I am today, I could not ask for a better support system. My family has always fostered a love for learning in me since I was younger and have encouraged me to push myself as much as possible in all things I do. When times have been difficult my family and friends have always been there for me to help me get to the other side. I am so incredibly thankful to have so many wonderful people in my life.

Chapter 2 is a version of D.W. Bradbury, J.T. Trinh, M.J. Ryan, C.M. Cantu, J. Lu, F.D. Nicklen, Y. Du, R. Sun, B.M. Wu, and D.T. Kamei. *On-Demand Nanozyme Signal Enhancement at the Push of a Button for the Improved Detection of SARS-CoV-2 Nucleocapsid Protein in Serum.* Analyst, 2021, 146: 7483-7490, doi: 10.1039/d1an01350e. Royal Society of Chemistry © 2021 Reprinted with permission from Royal Society of Chemistry. D. T. Kamei was the director of research for this article. This project was supported by the UCLA Technology Development Group & School of Medicine and by the National Science Foundation (NSF) Grant 1707194. C.M. Cantu would like to thank the National Institutes of Health (NIH) UCLA Maximizing Student Development (MSD) Program R25GM055052 for her research scholarship.

Chapter 3 is a version of D.W. Bradbury, J.T. Trinh, M.J. Ryan, K.J. Chen, A.A Battikha, B.M. Wu, and D.T. Kamei. *Integration of the Lateral-Flow Immunoassay with Multicolor Gold Nanorod Etching for the Semi-Quantitative Detection of Digoxin*, which is in preparation for

submission. D. T. Kamei was the director of research for this article. This project was supported by a seed grant provided by the Precise Advanced Technologies and Health Systems for Underserved Populations (PATHS-UP) Engineering Research Center (ERC) funded by the National Science Foundation (NSF) (Award No. 1648451).

Chapter 1. Motivation and Background

1.1. Introduction

1.1.1. Point-of-Care Diagnostics

Globally, there is a disproportionate burden of communicable and noncommunicable diseases on developing countries[1] with more than 95% of deaths due to infectious diseases occurring in these countries.[2] With adequate testing, many of the detrimental effects of these infectious diseases can be avoided leading to better health outcomes.[3] Therefore, researchers have focused on rapid, low-cost, point-of-care (POC) diagnostic devices that can be used in resource-limited settings to achieve better health outcomes. However, the benefits of rapid, low-cost tests are not limited to the detection of infectious diseases. Rapid testing for the early detection of noncommunicable diseases, which make up 7 out of the 10 leading causes of death worldwide and 80% of all deaths worldwide, allows for early intervention and better health outcomes.[1,4]

While current laboratory-based gold standard assays for diagnostics—such as real-time polymerase chain reaction, enzyme-linked immunosorbent assay (ELISA), etc.—can return accurate results, they have a long time to result and require trained personnel and expensive laboratory equipment, making them inaccessible to many resource-limited settings where the use of these diagnostics is critical. There has been increased focus on developing low-cost, POC-friendly diagnostics that meet the World Health Organization's ASSURED criteria: Affordable, Sensitive, Specific, User-friendly, Rapid and Robust, Equipment-free, and Deliverable.[5]

1.1.2. The Lateral-Flow Immunoassay (LFA)

One device that satisfies these criteria is the LFA. The LFA is a paper-based diagnostic device that utilizes capillary action, colorimetric indicators (commonly gold nanoparticles), and

immobilized primary antibodies to generate a binary output of whether the target antigen is present or not. The conventional LFA consists of four main regions as shown in **Figure 1.1**.

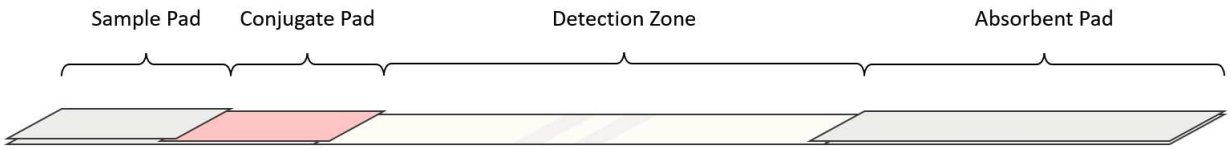

Figure 1.1. The setup of a conventional LFA. The LFA consists of a fiberglass sample pad, fiberglass pad with dehydrated conjugates, nitrocellulose detection region, and cotton linter absorbent pad.

The sample is introduced to the sample pad before flowing up the test strip. First, it flows into the conjugate pad, where it rehydrates the antibody-conjugated particles dehydrated in that region. The sample will then flow into the nitrocellulose detection region which contains the test and control lines. Lastly, the sample solution will flow into the absorbent pad, which serves to drive fluid flow through the entire test strip.

The conventional LFA has two main formats: the sandwich format and the competitive format. In the sandwich format (**Figure 1.2A**), the test line consists of primary antibodies against the target biomarker. As the sample flows through the detection region, sandwich-like complexes are formed as both the primary antibodies conjugated to the colorimetric indicators and the primary antibodies on the test line will bind to the target antigen. Any colorimetric indicators that do not form these sandwich-like complexes will flow past the test line and be bound by the control line, which consists of secondary antibodies that target the primary antibodies conjugated to the colorimetric indicators. Thus, in the case of a positive test, the sandwich LFA generates two visible lines, and in the case of a negative test, there is only the generation of a single visible control line.

If the control line is not present, it means the test is invalid and should be re-administered since the fluid did not flow up the strip.

In a competitive assay setup (**Figure 1.2B**), the test line consists of the target antigen itself. As the sample flows through the detection region, the target antigen in the sample will bind to the primary antibodies conjugated to the colorimetric indicators. As the colorimetric indicators flow past the test line, any free antibody binding sites on the colorimetric indicators will bind to the target antigen printed on the test line. Like the sandwich format, the control line consists of secondary antibodies which will bind any colorimetric indicators that did not bind to the test line. For a competitive assay, when the target antigen is present at high enough concentrations, the primary antibodies on the surfaces of the colorimetric indicators will be fully saturated and none of them will be able to bind to the test line. Therefore, a positive test is indicated by the presence of only one visible line at the control line, while a negative test is indicated by two visible lines. Once again, if the control line is not present, it means the test is invalid and should be re-administered.

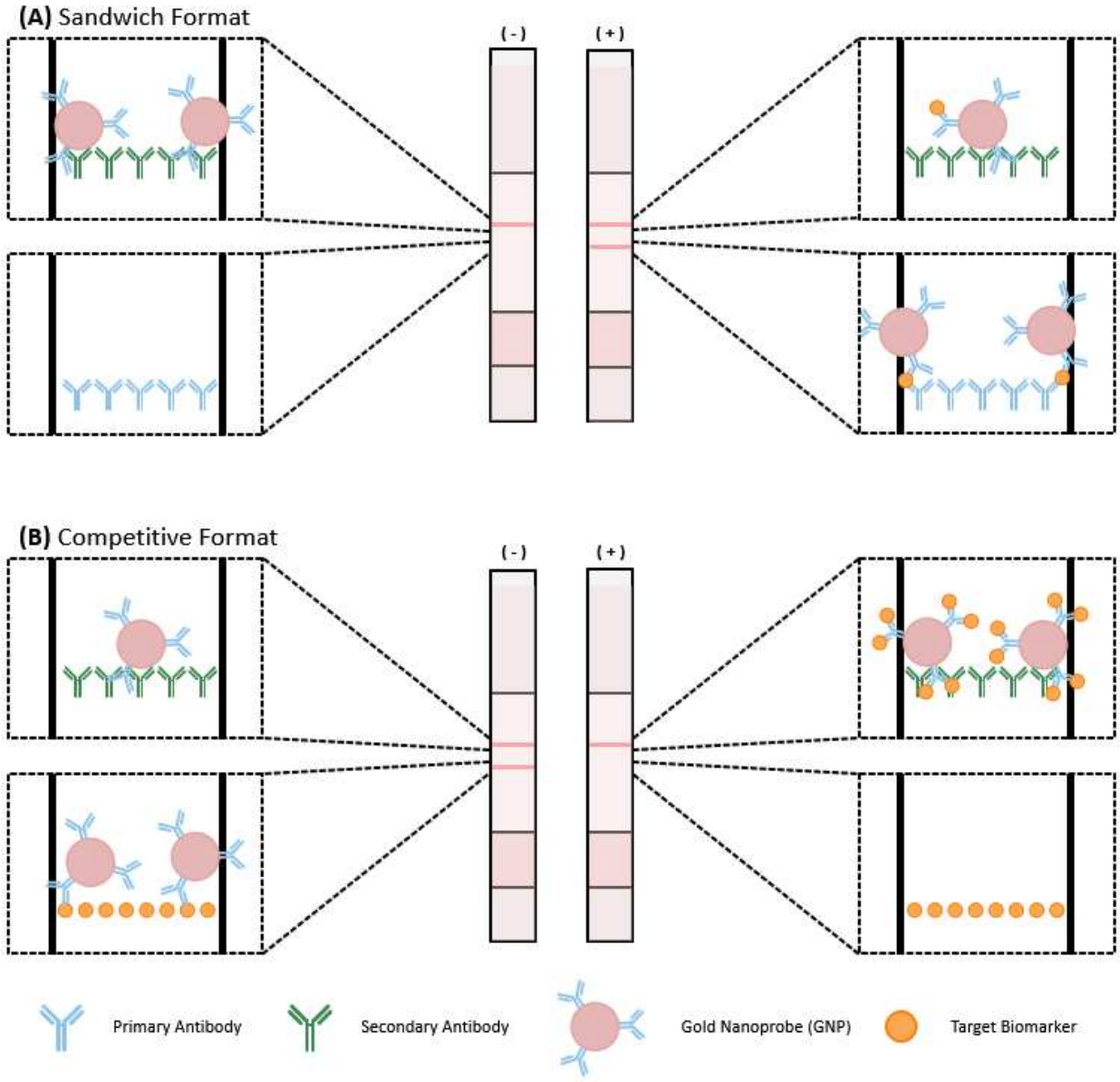

Figure 1.2. General schematics of the two formats of the LFA. (A) A negative (-) and positive (+) LFA using the sandwich format. (B) A negative (-) and positive (+) LFA using the competitive format.

While the LFA meets the World Health Organization's ASSURED criteria for a POC diagnostic, it also has some drawbacks. The LFA has a limited sensitivity and only returns a qualitative output on whether the target biomarker is present in the sample. Therefore, the

conventional LFA may not be useful for target biomarkers that are either present at extremely low concentrations or that require a quantitative output for diagnostic purposes.

To enhance the sensitivity of the LFA, researchers have used various methods such as a multi-conjugate system,[6] copper[7] and silver deposition,[8,9] and enzyme-based oxidation reactions.[10] To achieve a quantitative output, barcode-style LFAs [11–14] and electronic readers to interpret test line signals [15–23] have been developed.

In this thesis, I focus on improving the conventional LFA output by using colorimetric indicators that exhibit enzymatic activity. In Chapter 2, we use these enzymatic nanoparticles to improve the sensitivity of the LFA by utilizing a secondary reaction with the chromogenic substrate 3,3',5,5'-tetramethylbenzidine (TMB) to increase the resulting signal intensity. In Chapter 3, we achieve a semi-quantitative multicolor readout that is interpretable by the naked eye by incorporating enzymatic nanoparticles and the anisotropic etching of gold nanorods (GNRs) with the conventional LFA setup.

1.2. Introduction to Nanozymes

Nanoparticles that exhibit enzymatic activity are commonly referred to as nanozymes. It has been shown that noble metal nanoparticles exhibit pH-switchable enzymatic activity.[24] When introduced to an acidic environment, these noble metal nanozymes exhibit peroxidase-like activity, converting any hydrogen peroxide into free radicals.[25] This reaction can be used to oxidize a chromogenic substrate, such as TMB, to produce a visible signal output.[25] Conversely, when introduced to basic environments, these pH-switchable nanozymes exhibit catalase-like activity that decomposes hydrogen peroxide into water and oxygen.[26]

Nanozymes also have several advantages over enzymes for use in a POC diagnostic. Nanozymes are simpler and less expensive to synthesize than their enzymatic counterparts and can be more easily mass produced.[27] Additionally, nanozymes are more stable and robust than enzymes, since enzymes require the maintenance of specific conditions to maintain their functionality which may not always be achievable for POC devices targeted for resource-limited settings. These advantages make nanozymes a preferable alternative to natural enzymes when catalytic activity is necessary in a POC diagnostic such as the LFA.

1.3. Approaches Towards Signal Enhancement of the LFA

Many researchers have attempted to increase the sensitivity of the LFA without using expensive equipment to maintain its usefulness in resource-limited environments. To do so, researchers have explored various routes to increase the resulting test line signal intensity and thereby improve the sensitivity of the LFA. Some researchers have explored creating a multi-particle complex at the test line between the conventional detection probe and a secondary particle via a linking interaction.[6] In the work by Shen and Shen, researchers utilized the biotin-streptavidin interaction to create a dual-conjugate complex that led to a 30-fold improvement in detection over the conventional single-conjugate LFA.

Another approach to signal enhancement involves deposition of metals like copper and silver onto the surface of conventional gold nanoparticles.[7–9] In this method, the detection step proceeds as normal, and afterwards an enhancement solution, containing a reducing agent and the metal ions, is introduced to the LFA. The deposition of this metal is then catalyzed by any bound gold nanoparticles on the test or control line leading to increased signal intensity. In the work by

Tian *et al.*, researchers obtain a 100-fold to 1000-fold improvement in the limit of detection as compared to the conventional LFA.[7]

Other researchers have explored conjugating enzymes, such as horseradish peroxidase (HRP), to the surface of conventional colorimetric indicators.[10] In this technique, the detection step is allowed to run uninterrupted, and afterwards, a solution containing a chromogenic substrate is introduce to the LFA. When these substrates flow past the enzyme-conjugated detection probes bound to the test and control lines, they are oxidized leading to enhanced signals.

1.4. Approaches Towards Quantitative Outputs with the LFA and ELISA

1.4.1. Electronic Readers and the LFA

Researchers have developed electronic readers that can interface with the LFA to interpret the test line signal intensity to obtain a quantitative readout. These electronic readers can measure various LFA output signals including the standard visible output[15] as well as fluorescent,[16–19] chemiluminescent,[20] magnetic,[21] surface-enhanced Raman scattering (SERS),[22] and electrochemical signals.[23] While incorporating these readers with the LFA leads to much more sensitive tests, they often require trained personnel to quantify the outputs, and some of the equipment necessary to interpret these signals can be relatively expensive. These issues are therefore a major drawback when trying to use electronic readers to develop POC diagnostics.

1.4.2. Barcode-Style LFA

Alternatively, researchers have explored altering the LFA output to generate a semi-quantitative reading without the need for expensive equipment or trained personnel. One commonly used approach is the barcode-style LFA.[11–14] The barcode-style LFA consists of

multiple test lines against the same target, and the number of visible test lines can be correlated with target concentrations. As a result, an untrained user can compare the number of visible test lines to an included reference card to determine the concentration range of the target. This simple, one-step test generates rapid semi-quantitative results without the need for trained personnel or expensive lab equipment. However, there is a practical limit to the number of test lines that can be printed along the length of a standard LFA strip.

1.4.3. Conventional ELISA

When discussing the LFA, the commonly used comparative technology is the ELISA. While the ELISA requires trained personnel and expensive lab equipment and can have a long time to result, its high sensitivity makes it the gold standard laboratory diagnostic by which LFA performance is compared. Similar to the LFA, the ELISA detects the target via antibody-antigen interactions. There are three main formats of the ELISA: direct, indirect and sandwich (**Figure 1.3**).

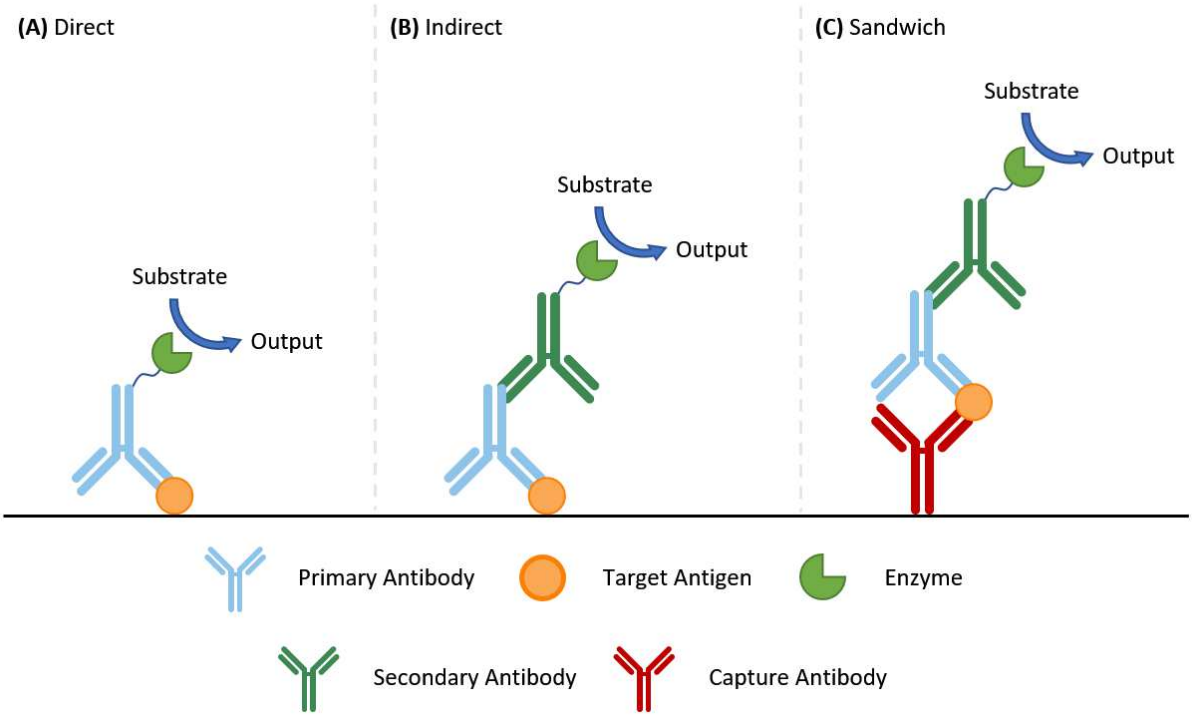

Figure 1.3. The three formats of the ELISA: direct, indirect, and sandwich.

Regardless of the format, a chromogenic substrate, such as TMB, is introduced to the well after the detection step. This substrate is then oxidized by the enzyme, usually HRP or alkaline phosphatase, conjugated to either the primary antibody (direct format) or the secondary antibody (indirect or sandwich format). Subsequently, a stop solution is added, and the optical density (OD) of the well is measured. The ELISA can be used either qualitatively or quantitatively. To run it quantitatively, a standard curve is generated using samples of known concentration which an unknown sample is then compared against.

1.4.4. Plasmonic ELISA (pELISA)

The conventional ELISA requires expensive lab equipment to measure the OD of the resulting wells which limits its applicability for resource-limited settings. As a result, researchers

have looked to develop an assay readout that is interpretable by the naked eye to remove the need for expensive equipment to quantify the output.

To do so, researchers have made use of the special optical properties of metallic nanoparticles. Metallic nanoparticles exhibit localized surface plasmon resonance (LSPR). When incident light interacts with a metal nanoparticle that is smaller than its wavelength, the surface electrons become excited and oscillate collectively at specific resonance frequencies.[28] This phenomenon is incredibly sensitive to several factors including metal nanoparticle size and shape, composition, spacing between separate particles, and refractive index of the surrounding dielectric media.[29] These factors were then utilized to develop the four main mechanisms of pELISA: triggering nanoparticle aggregation,[30,31] altering the refractive index in the nanoparticles' surroundings,[32,33] increasing the nanoparticle size,[34,35] and transforming the nanoparticles' shape or composition.[36–39]

With regard to altering the shape, pELISAs have been developed that functioned by altering the shape of gold nanorods (GNRs) to produce a multicolor readout.[36,37] Gold nanorods like all metal nanoparticles exhibit an LSPR. However, due to their cylindrical shape, GNRs express two distinct LSPR peak wavelengths: one longitudinally and another transversely.[40] The resulting color of the GNRs is controlled by their aspect ratio. When introduced to an oxidizing agent, GNRs undergo anisotropic etching at their ends to generate a color change that is detectable by the naked eye.[36,37]

To generate a multicolor output using the pELISA and GNRs, the detection step with enzymes conjugated to antibodies proceeds similar to the conventional ELISA. Subsequently, unlike the typical ELISA, the enzyme-conjugated antibodies generate oxidizing agents at a

concentration proportional to the target antigen concentration. The GNRs are then introduced and are anisotropically etched to a degree dictated by the oxidizing agent concentration. The color of the resulting suspension can be interpreted by the naked eye to obtain a quantitative readout of the initial antigen concentration.

1.5. Concluding Remarks and Thesis Overview

Although the LFA has many features that make it attractive for POC diagnostic use in resource-limited settings, its low sensitivity and lack of quantitative results make it unsuitable for certain applications. While research has been conducted to both increase the sensitivity of the LFA and introduce a quantitative readout, this work primarily utilizes equipment and trained personnel, preventing accessibility in resource-limited settings. This thesis focuses on the introduction of enzymatic activity into the conventional LFA through the use of nanozymes to achieve both increased sensitivity and a quantitative readout without the need for expensive external equipment.

In Chapter 2, we developed a 3D printed casing that contains an LFA, dehydrated enhancement reagents, and an enhancement buffer reservoir. At the push of a button, this device can achieve nanozyme-mediated enhancement of the LFA to detect the SARS-CoV-2 nucleocapsid protein (N-protein) at concentrations as low as 0.1 ng/mL in just 40 min. It is a version of D.W. Bradbury, J.T. Trinh, M.J. Ryan, C.M. Cantu, J. Lu, F.D. Nicklen, Y. Du, R. Sun, B.M. Wu, and D.T. Kamei. *On-Demand Nanozyme Signal Enhancement at the Push of a Button for the Improved Detection of SARS-CoV-2 Nucleocapsid Protein in Serum.* Analyst, 2021.

In Chapter 3, we focused on achieving a quantitative output with the LFA without the need for expensive equipment. To do so, we utilized the catalase-like activity of a platinum-based nanozyme to integrate the conventional LFA workflow with the anisotropic etching of GNRs. This

multicolor, semi-quantitative assay was able to detect the cardiac glycoside digoxin in human serum within the relevant therapeutic range of 0.5 to 3 ng/mL. It is a version of D.W. Bradbury, J.T. Trinh, M.J. Ryan, K.J. Chen, A.A Battikha, B.M. Wu, and D.T. Kamei. *Integration of the Lateral-Flow Immunoassay with Multicolor Gold Nanorod Etching for the Semi-Quantitative Detection of Digoxin*, which is in preparation for submission.

Chapter 2. On-Demand Nanozyme Signal Enhancement at the Push of a Button for the Improved Detection of SARS-CoV-2 Nucleocapsid Protein in Serum

2.1. Introduction

The severe acute respiratory syndrome coronavirus 2 (SARS-CoV-2) has caused an ongoing and devastating pandemic which remains a major threat to global public health.[41,42] The nucleocapsid protein (N-protein) is a major structural protein of coronaviruses which is involved in the packing of RNA within the virus. It is highly conserved between coronaviruses, with the SARS-CoV and SARS-CoV-2 N-proteins sharing 90% homology.[43] During the first week of infection, the N-protein is shed at relatively high concentrations into nasopharyngeal fluid and serum.[44] It has previously been utilized to diagnose SARS-CoV infections, where the viral N-protein could be detected as early as 1 day after onset of symptoms in a variety of different bodily fluids.[45] Recent studies have shown that patients in the early stages of infection with SARS-CoV-2 also have detectable circulating N-protein in serum.[46,47] Due to its functional significance to coronaviruses and its abundance in bodily fluids, it has been suggested that the N-protein in serum could serve as an antigen target for early SARS-CoV-2 detection.

An at-home diagnostic would allow for more widespread rapid detection of initial infection in a low-cost manner, which would allow patients to be treated and quarantined to prevent further outbreaks. This is especially important as the current gold standard for detecting SARS-CoV-2 is reverse transcription real-time PCR, which requires samples to be sent to laboratories that have equipment, power, and trained personnel. This leads to a delay in the individual receiving results and therefore potential for continued transmission of the virus.[48] Lateral-flow immunoassays (LFAs) exhibit many of the characteristics desired for point-of-care diagnostics and can easily be

performed at home with the correct sampling method. The most common application of LFAs is the over-the-counter pregnancy test. Having a similar rapid, inexpensive, and easy-to-use test for SARS-CoV-2 will lead to widespread screening of healthy, asymptomatic, and symptomatic individuals. This blanket screening approach will play a significant role in allowing society to return to normal while maintaining safety.

Several LFAs that directly detect the spike protein and N-protein within the first week of infection have become commercially available during the pandemic through the FDA's Emergency Use Authorization.[49–51] It is important to note that all of the antigen-based LFAs currently available use nasal and/or nasopharyngeal swabs for sample collection. While the use of a nasopharyngeal swab has greater potential to sample and capture virus due to the localization of SARS-CoV-2 in the upper respiratory tract, it requires some level of guidance to ensure proper sample collection and thus is not ideal for at-home testing. Both swabbing collection methods are also prone to user error and variation depending on how the user inserts the swab into the nasal cavity. In fact, swabbing variability has been shown to impact even highly sensitive laboratory diagnostics for SARS-CoV-2.[52,53] Additionally, nasal and nasopharyngeal swabs must be significantly diluted into a buffer before being utilized in any LFA-based diagnostic. These disadvantages cause the nasal and nasopharyngeal swabs to be less-than-ideal sample collection methods for an at-home diagnostic.

In contrast, sample fluids such as blood, serum, and saliva can be utilized and are easier to collect consistently. However, they cannot be used with the currently available LFA technology due to having lower viral loads or antigen concentrations than those in nasopharyngeal samples. Li and Lillejoh recently reported the development of the first smartphone-based, microfluidic point-of-care device for the sensitive quantification of N-protein in serum down to 0.1 ng/mL.

While able to detect low levels of N-protein, this assay requires the user to perform multiple reagent addition steps and possess a smartphone, potentially limiting its applicability for self-testing and widespread use in low resource regions.[54] An alternative approach is to develop a more sensitive version of the LFA which maintains its ease-of-use and equipment-free characteristics while also being able to detect low levels of N-protein in blood. Some common techniques to improve LFA sensitivity involve biomarker preconcentration and signal enhancement.[55,56]

While gold nanoparticles are the most widely used detection probes for LFAs, other probes such as magnetic nanoparticles, carbon nanoparticles, quantum dots, luminescent nanoparticles, and colored latex have been used to improve sensitivity or provide additional functionalities.[57–62] In this work, we use platinum-coated gold nanozymes (PtGNs) for their demonstrated ability to exhibit peroxidase-like activity at acidic pH levels.[63] Previously, our lab has used this peroxidase-like activity to introduce a purple 3,3',5,5'-tetramethylbenzidine (TMB) precipitate to enhance the LFA signal.[56] For this device, the reagents required for this process are dehydrated to make them more suitable for an at-home test.

In this work, we developed a novel paper-based device that incorporates an LFA test strip, dehydrated signal enhancement reagents (nanozymes and their associated chemicals), and a sealed chamber with stored liquid enhancement buffer in an innovative 3D printed casing. Our device enabled the detection of N-protein in undiluted serum in 40 min at concentrations as low as 0.1 ng/mL, which was at least a 10-fold improvement over the conventional LFA. Moreover, with this all-in-one device, only one simple step of pushing a single button is needed for the signal enhancement to occur after the LFA detection step.

2.2. Materials and Methods

2.2.1. Preparation of biotinylated anti-N-protein capture antibodies

All reagents and materials were purchased from Sigma-Aldrich (St. Louis, MO) unless otherwise noted. Biotinylated anti-N-protein capture antibodies were prepared by NHS-ester linkage using NHS-PEG-biotin. 15 µL of a 3 mM NHS-PEG-biotin solution was added to 50 µL of 0.5 mg/mL anti-N-protein antibodies (#40143-MM05, Sino Biological, Wayne, PA) in phosphate-buffered saline (PBS, pH 7.4) and reacted for 30 min, allowing the NHS-PEG-biotin to conjugate onto the free surface primary amines of the antibodies. The conjugation reaction was stopped via buffer exchange in fresh PBS using Zeba Spin Desalting Columns (Fisher Scientific, Waltham, MA).

2.2.2. Preparation of anti-N-protein detection antibody decorated platinum-coated gold nanozyme probes (anti-N-protein PtGNPs)

Platinum-coated gold nanozymes were synthesized using a protocol derived from Gao et al.[63] Briefly, 4 mL of 40 nm citrate-capped gold nanoparticles (GNs) (Nanocomposix, San Diego, CA) and 1686 µL of filtered ultrapure water were preheated to 90°C in an oil bath under magnetic stirring for 20 min. Following the preheating, 314 µL of a 0.82 mM chloroplatinic acid hydrate solution and 2 mL of a 3.3 mM ascorbic acid solution were injected separately into the gold nanoparticle suspension using a syringe pump at rates of 0.6 and 1.2 mL/h, respectively. The reaction was allowed to proceed for 1 h after the injection was complete.

To create anti-N-protein decorated platinum-coated gold nanozyme probes (anti-N-protein PtGNPs), 30 µL of a 0.1 M sodium borate solution (pH 9) was first added to 1 mL of PtGNs. Then, 4 µg of primary anti-N-protein antibody (#40143-R001, Sino Biological, Wayne, PA) was added

to the suspension and incubated for 30 min at room temperature (22°C). 50 μL of a 10% (w/v) bovine serum albumin (BSA) in filtered ultrapure water solution was then added to the suspension and incubated for 10 min. Free antibodies were removed with three centrifugation cycles at 8600 RCF and 4°C for 6 min each. For the first two cycles, the pellet was resuspended in 200 μL of 1% (w/v) BSA in filtered ultrapure water, and the final pellet was resuspended to a final volume of 50 μL in 0.1 M sodium citrate buffer (pH 6).

2.2.3. Preparation of LFA test strip

The LFA test strips were composed of overlapping pads secured to an adhesive backing. These pads included a biotinylated-anti-N-protein antibody pad, an anti-N-protein PtGNP conjugate pad, a nitrocellulose membrane, and a CF4 absorbent pad (Cytiva, Marlborough, MA). To prepare the detection region of the LFA, proteins were first printed and immobilized on a Unisart CN140 nitrocellulose membrane (Sartorius, Göttingen, Germany) using an Automated Lateral Flow Reagent Dispenser (Claremont BioSolutions LLC, Upland, CA) with the voltage setting at 4.5 V and a Fusion 200 syringe pump (Chemyx Inc, Stafford, TX) with a flow rate of 300 μL/min. The test line was formed by printing a solution of a 2 mg/mL polystreptavidin (Biotez, Berlin, Germany) solution in 25% (w/v) sucrose. The control line was formed by printing a solution of 0.25 mg/mL goat anti-rabbit IgG secondary antibody in 25% (w/v) sucrose. The printed membrane was left in a vacuum-sealed desiccator overnight and subsequently stored in a bag containing Drierite desiccant (W.A Hammond Drierite Co, Xenia, OH) for an additional day.

To create each nanozyme conjugate pad, 6 μL of anti-N-protein PtGNPs were diluted to form a 20 μL solution with final concentrations of 5% (w/v) trehalose and 1% (w/v) BSA and then dehydrated onto a 5 mm × 10 mm piece of Standard 17 fiberglass paper (Cytiva, Marlborough,

MA). The conjugate pads were dehydrated in a desiccator at 37°C overnight. To create each capture antibody pad, 2 µL of a 0.05 mg/mL biotinylated anti-N-protein capture antibody solution was diluted to form a 20 µL solution with final concentrations of 5.74% (w/v) trehalose and 1.15% (w/v) BSA and then dehydrated onto a 5 mm × 10 mm piece of fiberglass paper. The pads were dehydrated in a vacuum-sealed desiccator overnight.

To assemble the LFA test strip, the nitrocellulose membrane was first adhered to an adhesive backing. Individual strips were cut to be 5 mm in width. To each strip, a CF4 absorbent pad was placed on the adhesive backing downstream of the control line, overlapping the nitrocellulose membrane by 3 mm. The PtGNP conjugate pad was placed on the adhesive backing upstream of the test line, overlapping the nitrocellulose membrane by 2 mm. The biotinylated capture antibody pad was placed on the adhesive backing upstream of and overlapping the PtGNP conjugate pad by 1 mm.

2.2.4. Design and assembly of device for enhancement reagent storage and delivery on LFA

A casing was designed to eliminate the need for multiple liquid- and test strip-handling steps. This 3D printed device provides in-test liquid reagent storage, dehydrated enhancement reagents, and movable paper architecture that directs the flow of liquid through the LFA test strips. The three major components of the device are outlined in **Figure 2.1**. The parts shown in gray were 3D printed using an Ultimaker 3 FDM 3D printer (Ultimaker B.V., Geldermalsen, Netherlands) out of Ultimaker CPE filament (co-polyester).

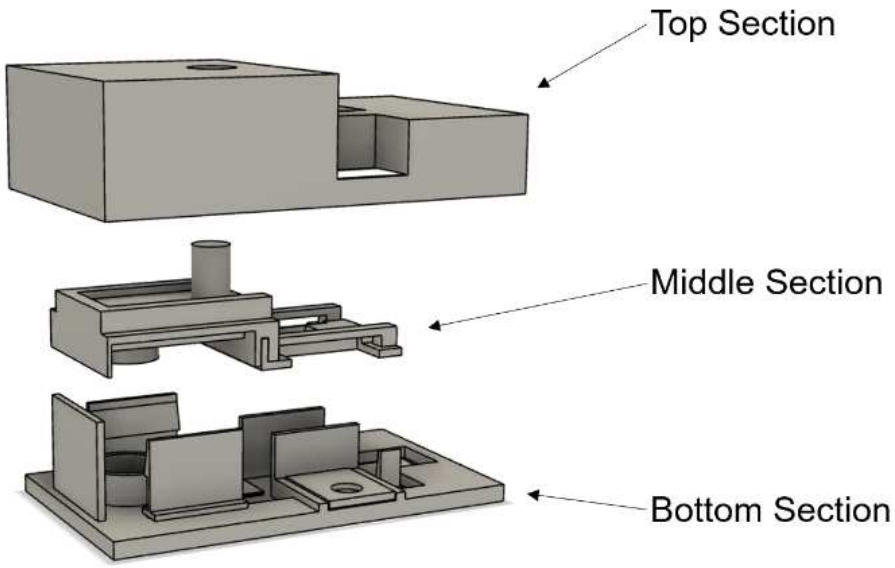

Figure 2.1. Design of the three main casing pieces for nanozyme signal enhancement of the LFA.

The bottom piece of the casing, along with the inserted paper pads and test strip, are detailed in **. Overview of the bottom piece of casing.** (Left) Labelled CAD drawing of bottom piece of casing. (Right) Photograph of 3D printed bottom piece of casing with LFA test strip and enhancement reagent paper pads in position.. The enhancement buffer release well is an enclosed, hollow cylinder with a dome in the center. The dome serves to rupture a foil sealed buffer reservoir on the middle piece of the casing. 0.05 g of urea hydrogen peroxide was sprinkled in the hollow cylinder surrounding the dome and then covered with a ring of fiberglass paper. A 62.5 μL solution of 6.5 mM TMB, 15% (w/v) trehalose, and 20% (w/v) dimethylformamide in 0.1 M sodium citrate buffer (pH 5) was dehydrated onto a 13 mm × 12 mm fiberglass pad overnight in a vacuum sealed desiccator to create the TMB pad. The enhancement reagent absorbent pad is composed of a 13 mm × 23 mm CF4 absorbent pad. The four aligning snap fit joints hold the middle piece of the casing in a lifted position until the user presses down on it. When pressed, the middle piece then

snaps into place and is held down in a constant position by the snap fit joints. The bottom piece also contains a sample well which is located above the biotinylated capture antibody pad when the device is fully assembled.

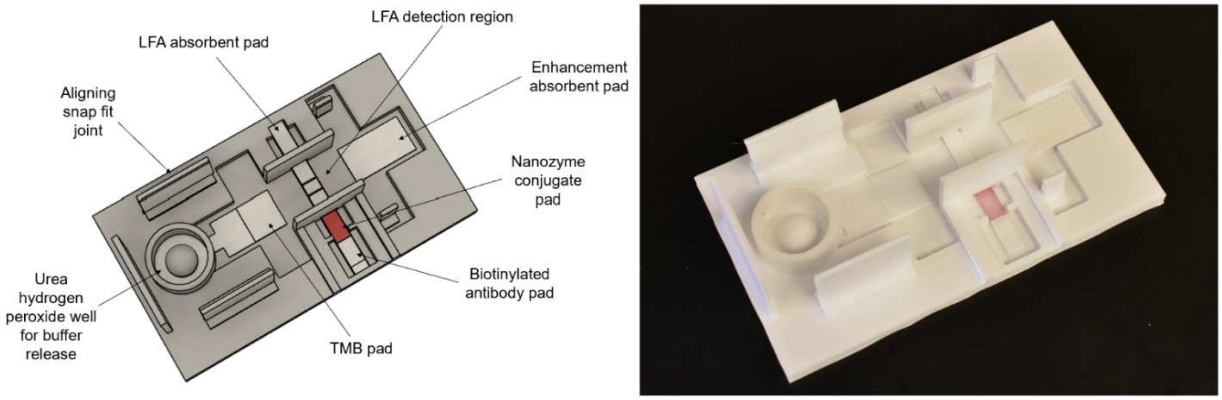

Figure 2.2. Overview of the bottom piece of casing. (Left) Labelled CAD drawing of bottom piece of casing. (Right) Photograph of 3D printed bottom piece of casing with LFA test strip and enhancement reagent paper pads in position.

The movable middle piece of the casing, shown in **Figure 2.3**, contains the enhancement buffer reservoir and two connector pads. The left pad is made up of Standard 17 fiberglass paper while the right pad is a CF4 absorbent pad. The enhancement buffer, which will solubilize the urea hydrogen peroxide and TMB during the assay, was stored within the reservoir of the middle piece. To fill the reservoir, 600 µL of 1% (w/v) dextran sulfate in 0.1 M sodium citrate buffer (pH 5) was pipetted into the reservoir. To seal the liquid in the reservoir, a sheet of mylar foil was placed on top of the reservoir and heat was applied using a hot iron for 3 s followed by complete cooling. The top piece of the casing serves to help hold the other components in place and protect them from external and environmental factors. It also contains a viewing window to observe the detection results (**Figure 2.4A**).

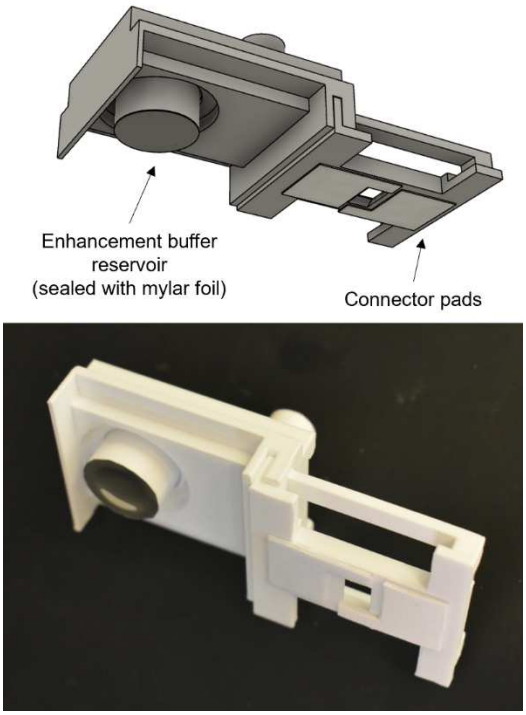

Figure 2.3. Overview of the middle piece of the casing. CAD drawing (top) and 3D printed piece (bottom) showing the underside view of the middle piece of the casing and the locations of the enhancement buffer fluid reservoir and the paper connector pads.

2.2.5. Detection of N-protein in human serum with nanozyme signal enhanced LFA

To detect for N-protein using our nanozyme signal enhanced LFA, a 25 μL human serum sample (#50-203-6415, Fisher Scientific, Waltham, MA) spiked with varying concentrations of N-protein (#40588, Sino Biological, Wayne, PA) was added to the sample well on the LFA (above the biotinylated capture antibody pad). As in the case of typical LFAs for serum samples, this was immediately followed by a chase buffer. In our system, we used 75 μL of chase buffer composed of 2% (w/v) polyvinylpyrrolidone 10kDa, 0.2% (w/v) BSA, 0.2% (w/v) Tween 20, and 0.2% (w/v) casein in 0.1 M potassium phosphate at pH 7.2. After 20 min, the user pressed the button to move down the middle piece of the casing (**Figure 2.4B**). The movement of the middle casing piece

resulted in the rupture of the mylar seal to release the enhancement buffer and also served to lower the connector pads to provide a continuous flow path for the enhancement reagents to flow through the LFA strip. Final results were observed after 20 min of enhancement. Results were photographed before and after the signal enhancement reaction with a Nikon D3400 digital camera (Nikon, Tokyo, Japan) in a controlled lighting environment. To quantify the relative test line intensities, the resulting images were processed by a MATLAB script developed by our lab.[64]

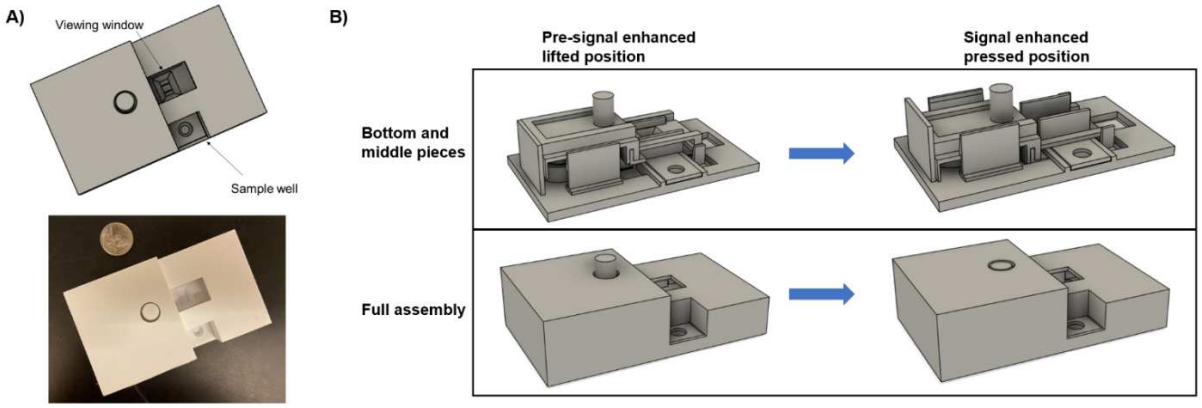

Figure 2.4. Overview of the fully assemble casing and button pressing mechanism. (A) CAD drawing (top) and 3D printed (bottom) full casing assembly with labelled viewing window and sample well. US quarter included for size comparison. (B) CAD drawings showing the casing before and after pressing the middle piece.

2.2.6. Cross-reactivity tests with other N-proteins

To test for cross-reactivity of our device with the Middle East respiratory syndrome coronavirus (MERS-CoV) N-protein (#40068, Sino Biological, Wayne, PA) and human coronavirus 229E (HCoV-229E) N-protein (#40640, Sino Biological, Wayne, PA), the assay was run using the same steps as described in Section 2.6. Samples of SARS-CoV-2 N-protein, MERS-CoV N-protein, and HCoV-229E N-protein were tested at 1.0 ng/mL in human serum.

2.3. Results and Discussion

2.3.1. Demonstration of improved N-protein detection using nanozyme signal enhancement

The operation of our device for the nanozyme signal enhanced detection of N-protein occurs in two main steps. The first is the antigen capture and detection step and the second is the signal enhancement step (**Figure 2.5**). The user first applies the serum sample to the sample well immediately followed by the addition of the chase buffer. The liquid will first resolubilize the biotinylated capture anti-N-protein antibody and then the anti-N-protein PtGNPs. In the case of a positive sample, these antibody species will bind to any N-protein in the sample resulting in the formation of sandwich complexes. As these complexes flow through the LFA strip, they will be captured at the test line due to the strong biotin-streptavidin interaction between the biotinylated capture antibody and the streptavidin immobilized on the test line. This will ultimately result in the capture of PtGNPs at the test line region. In the case of a negative sample where no N-protein is present, no sandwich complex will form. Therefore, even though the biotinylated capture antibody will bind to the streptavidin at the test line, no PtGNPs will be captured. Regardless of the sample being positive or negative for N-protein, any PtGNPs that do not get captured at the test line will be able to be captured by the secondary antibody at the control line to indicate that the sample flowed properly through the test strip.

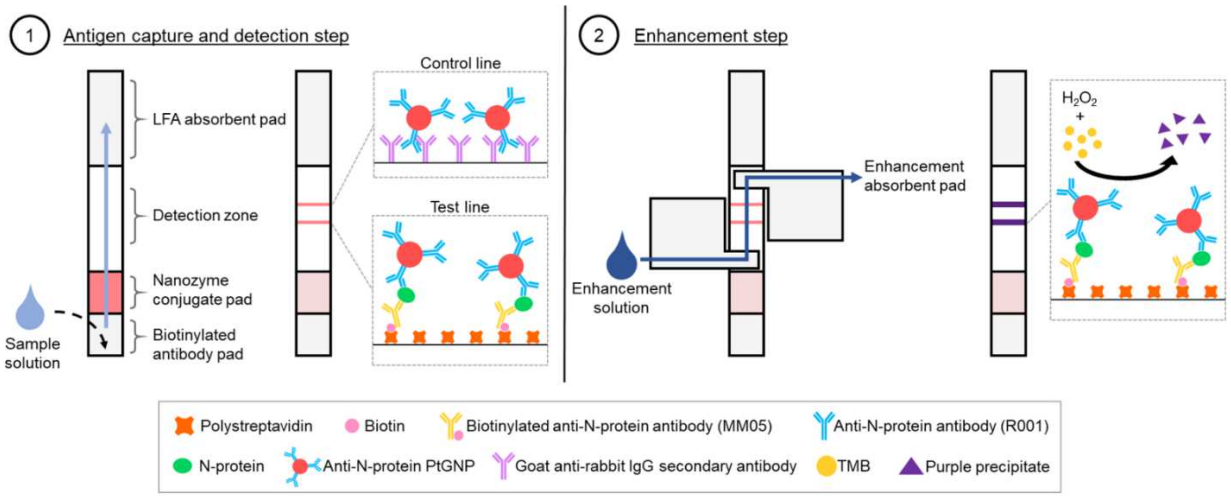

Figure 2.5. Simplified schematic of assay steps and paper segments touching the LFA test strip. (1) Sample is applied to the sample well above the test strip where biotinylated antibody and PtGNPs are rehydrated and antigen capture occurs at the detection zone. (2) After pressing the button to move the middle piece of the casing down, enhancement buffer is released to rehydrate the dehydrated enhancement reagents and flow through the test strip resulting in signal enhancement at the detection zone.

After 20 min, instead of the typical signal enhancement process of a user creating a signal enhancement solution and then physically moving the LFA strip into that solution, the user will only need to press down on the button connected to the middle piece of the casing. This lowers the middle piece where it snaps into place with the connector pads bridging gaps between the dehydrated TMB pad and the LFA strip, as well as the LFA strip and the enhancement absorbent pad. Additionally, as the middle piece is lowered, the mylar seal on the enhancement buffer reservoir is ruptured by the dome, which allows the enhancement buffer to flow into the release well. Once released, the buffer solubilizes the urea hydrogen peroxide, followed by the TMB. This enhancement solution then flows through the LFA test strip and into the enhancement absorbent pad. As the solution passes the detection zone, any PtGNPs bound to the test line will catalyze the oxidation of TMB to TMB^+. The TMB^+ will complex with the negatively charged dextran sulfate, leading to the formation of an insoluble purple product that becomes deposited at the test line. This

results in the enhancement of the test line signal over an additional 20 min, improving the sensitivity of the LFA.

To evaluate the performance of this assay, we tested samples containing 0, 0.03, 0.1, 0.3 and 1 ng/mL of N-protein spiked into human serum. The final LFA strips from one of our experimental studies are shown in **Figure 2.6**. Before the enhancement step, a clearly visible test line is present at 1 ng/mL but not at 0.3 ng/mL, indicating a detection limit of 1 ng/mL. After enhancement, the test line at 1 ng/mL becomes significantly darker and a visible test line also appears at 0.1 and 0.3 ng/mL, demonstrating at least a 10-fold improvement in detection limit.

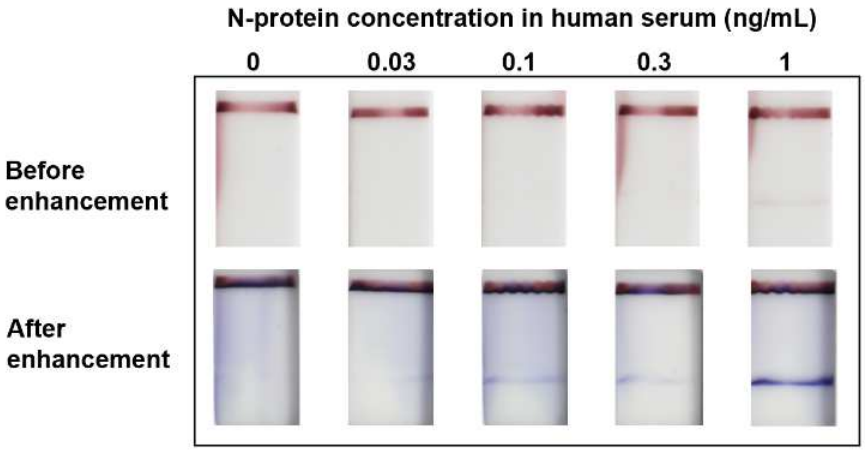

Figure 2.6. Detection of the N-protein of SARS-CoV-2 in human serum using nanozyme signal enhanced LFA. Detection limit before enhancement is 1 ng/mL while after enhancement it is 0.1 ng/mL, demonstrating at least a 10-fold improvement in detection limit and detection of N-protein within the desired concentration range.

This experimental study was performed four times. The relative test-line intensities were then quantified using a custom MATLAB script developed by our lab, and the results are shown in **Figure 2.7**. These results demonstrate the ability of our nanozyme signal enhanced assay to consistently detect for N-protein in serum down to 0.1 ng/mL. This is at least a 10-fold improvement over the 1 ng/mL result initially seen in the unenhanced LFA. This current detection

limit falls within the physiologically relevant range of serum N-protein concentrations reported for SARS-CoV-2.[45–47]

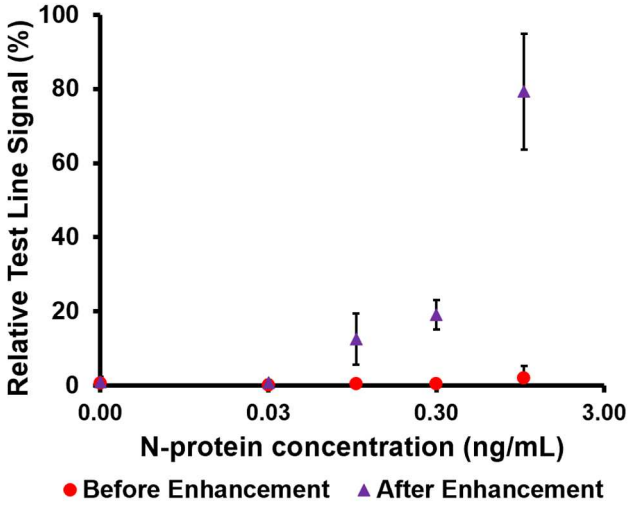

Figure 2.7. Plot of test line signal intensity. Plot of relative test line signal intensity versus N-protein concentration for both the LFA (red ●) and enhancement steps (purple ▲). Data is represented as the mean ± SD (n = 4).

Compared to current commercially available LFAs that rely on the high N-protein concentrations in nasal and nasopharyngeal fluids, our device can detect for the lower N-protein concentrations in serum. This makes our device compatible with serum, whose collection is more consistent and less prone to user error than using nasal or nasopharyngeal swabs.

Additionally, as the signal enhancement step requires only a single button push from the user, our device is able to achieve this improved sensitivity without the addition of any liquid and test strip handling steps or electronic devices. Comparing the results of our device to a recently developed smartphone-based microfluidic device, we achieve the same detection limit of 0.1 ng/mL despite our device not having any electronic components.[54]

Finally, with slight modifications, our signal enhanced assay would be suitable for the detection of N-protein in swab-based samples and could also be adapted for the detection of SARS-CoV-2 spike protein or other antigen targets.

While our device has a more complex construction than the conventional LFA, the casing can still be mass produced using injection molding processes and the test strips can be created using existing LFA diagnostic manufacturing infrastructure. Moreover, compared to other approaches to improve sensitivity such as the integration of electronic readers, our device is much less complex, making it easier to scale-up production and be more affordable to the end user.[65] The steps for operation are also not much more difficult than the conventional LFA, requiring just an additional press of a button.

2.3.2. Cross-reactivity tests with MERS-CoV and HCoV-229E N-proteins

To evaluate the cross-reactivity of our device, we ran our assay with N-proteins from the SARS-CoV-2, MERS-CoV, and HCoV-229E viruses at 1.0 ng/mL in human serum. Each test was performed three times. The unenhanced and enhanced LFA results, as well as a MATLAB analysis of the test line intensities, are provided in **Figure 2.8**. The results show clear detection of the SAR-CoV-2 N-protein and no cross-reactivity with the MERS-CoV and HCoV-229E N-proteins. While future sensitivity and specificity tests would be required before commercialization, the success of the cross-reactivity tests provides the initial steps towards functional evaluation of our device.

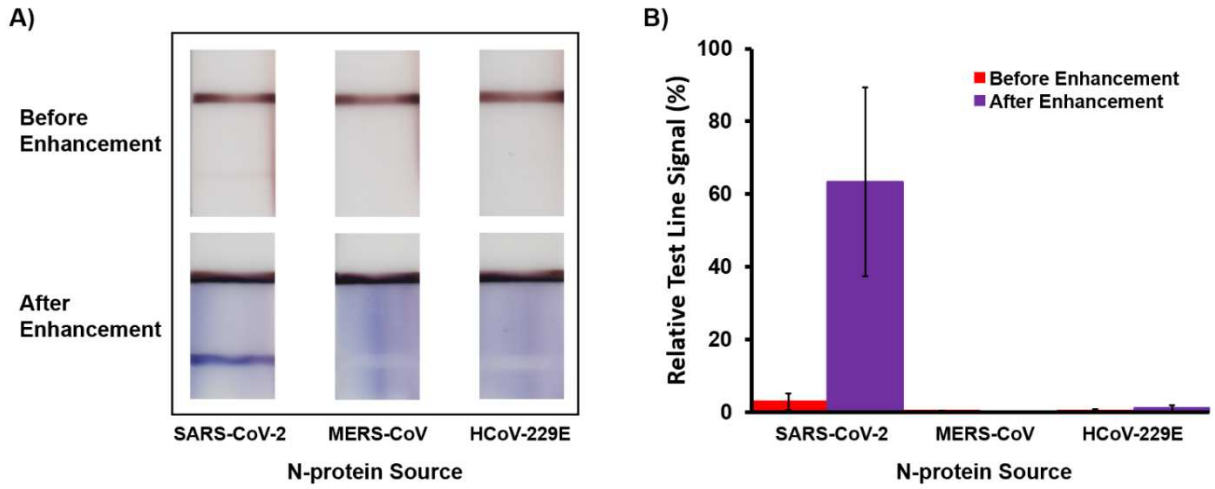

Figure 2.8. Results from cross-reactivity tests. (A) Results from cross-reactivity tests with MERS-CoV and HCoV-229E N-proteins, confirming that our assay has no cross-reactivity with the N-proteins from these viruses. Each N-protein was run at 1.0 ng/mL in human serum. (B) Plot of relative test line signal intensity for N-proteins from SARS-CoV-2, MERS-CoV, and HCoV-229E at 1.0 ng/mL in human serum. Data is represented as the mean ± SD (n = 3).

2.4. Conclusions

In summary, we have developed a nanozyme signal enhanced LFA for the improved detection of the N-protein of SARS-CoV-2 in serum. An innovative 3D printable casing was designed, which stored all assay components including the LFA test strip, dehydrated signal enhancement reagents, and a sealed chamber with stored liquid enhancement buffer. Our paper-based device was able to detect N-protein in undiluted serum in 40 min at concentrations as low as 0.1 ng/mL, which was at least a 10-fold improvement over the conventional LFA. Moreover, with this all-in-one device, only one simple step of pushing a single button is needed for the signal enhancement to occur after the LFA detection step. The development of devices that have the ability to detect for SARS-CoV-2 antigen biomarkers with improved sensitivity, while maintaining a user-friendly design and scalable manufacturing, is vital to increasing the frequency in screening asymptomatic individuals. This has the potential to significantly improve the response to the

COVID-19 pandemic by effectively detecting patients at their early stages of infection and allowing for effective treatment and quarantining procedures to be implemented.

Chapter 3. Integration of the Lateral-Flow Immunoassay with Multicolor Gold Nanorod Etching for the Semi-Quantitative Detection of Digoxin

3.1. Introduction

Heart disease, including atrial fibrillation (AF) and heart failure (HF), remains the leading cause of death for adults in the United States. It is expected that the number of individuals with AF in the United States will increase from 5.2 million in 2010 to 12.1 million by the year 2030.[66] Additionally, nearly 6.2 million adults in the United States live with HF and the number of cases is expected to surpass 8 million by the year 2030.[67] Consequently, HF costs the nation an annual $30.7 billion in healthcare services, medications, and missed days of work.[68] Furthermore, cardiovascular disease disproportionately affects underrepresented populations, which are often in areas with reduced healthcare access.[69]

One drug that is used in the treatment of HF and AF is the cardiac glycoside digoxin. Despite being the oldest and one of the most well-known drugs for the treatment of HF and AF, digoxin remains one of the most challenging cardiovascular therapies to administer properly. This is due to its narrow therapeutic window and the small difference between its therapeutic and toxic doses.[70] To address this issue, therapeutic drug monitoring is often employed to measure the blood plasma concentration of the drug and ensure that the trough level is within the therapeutic range of 1-2 ng/mL as opposed to the toxic concentration (>2.8 ng/mL).[71] If the measured concentration of digoxin in the blood is not within the desired range, the patient's next dose can be adjusted, thus providing a method of individualizing treatment. Typically, highly quantitative techniques, such as the enzyme-linked immunosorbent assay (ELISA), high performance liquid chromatography, or automated immunoassay systems, are utilized for monitoring cardiac drugs.[72–74] Despite their success in large hospital settings, these tests are not feasible for use in small mobile clinics residing

in underserved communities due to the requirement of highly expensive equipment, trained laboratory personnel, and a long time to result, especially if the sample has to be sent away to an offsite laboratory.[75]

One effort to make the ELISA more suitable for use in resource-limited settings was the development of the plasmonic enzyme-linked immunosorbent assay (pELISA).[76,77] In the pELISA, traditional chromogenic substrates are replaced with plasmonic nanoparticles. One mechanism involves coupling analyte capture with a reaction that controls the anisotropic etching of gold nanorods (GNRs).[36,37] Different concentrations of the target analyte result in GNRs of different aspect ratios and thus different colored suspensions. This produces a multicolor readout with a full spectrum of colors. Compared to the traditional ELISA, which generates a change in color intensity and thus requires expensive plate readers to interpret results, the pELISA generates a change in color hue. The results are easily interpreted with the naked eye by comparing the color development with a provided reference card (similar to litmus pH test strips). While effective at introducing a quantitative naked-eye readout to the ELISA, the pELISA still has a long time to result and requires trained personnel to perform many binding and washing steps, making it unsuitable for use at the point of care (POC). Therefore, there is still a need for a POC device that can perform quantitative therapeutic drug monitoring in underserved communities.

A POC device should be small and lightweight, require minimal power, training, and equipment, and also be low in cost. One device that satisfies these criteria is the lateral-flow immunoassay (LFA), a paper-based device that transports a sample via capillary action and uses colorimetric indicators conjugated with antibodies to visually detect the presence or absence of a target analyte. The most recognizable versions of the LFA are the over-the-counter pregnancy test and the COVID rapid antigen tests which have achieved widespread success in today's market due

to their ease of use and accurate, rapid results. Despite its success, the LFA still suffers from a few disadvantages which limit its ability to completely replace laboratory-based assays.[78] One disadvantage is that the conventional LFA only provides the user with a qualitative "yes" or "no" binary readout. For this reason, the traditional LFA is not appropriate in situations where a quantitative answer is required, such as therapeutic drug monitoring. Various approaches have been developed to introduce a more quantitative readout to the LFA, such as the barcode-style LFA[79–81] and electronic readers.[82–84] Although these approaches have been useful, the barcode-style LFA has a relatively poor quantitative resolution, while the requirement of electronic readers can increase the cost and complexity of an assay. Thus, there is still a need for inexpensive, easy-to-use, rapid assays that allow for naked-eye quantification of biomarkers at the POC.

In this work, we developed a technology that combines the LFA with the multicolor signal generation capabilities of the pELISA to improve the naked-eye quantitative capabilities of the LFA. Digoxin capture and binding occur on our modified LFA test strip which utilizes platinum nanozyme probes with catalase-like activity. This test strip is combined with a reaction that controls the oxidative, anisotropic etching of GNRs to produce a wide range of visible colors dependent on the initial digoxin concentration in the sample. We demonstrated the ability of this technology to be used for the naked-eye quantification of digoxin in human serum samples within the relevant concentration range of 0.5-3.0 ng/mL. To our knowledge, this is the first reported integration of the LFA with GNR etching, as well as the first multicolor LFA readout where the color produced is dependent on the concentration of the antigen analyte.

3.2. Materials and Methods

3.2.1. Synthesis of gold nanorods (GNRs)

All reagents and materials were purchased from Sigma-Aldrich (St. Louis, MO) unless otherwise noted. GNRs were synthesized in house using a modified version of the seeded growth method reported by Ye *et al*.[85] This method requires the preparation of both gold nanoparticle seeds and a growth solution. To make the seed suspension, 5 mL of 0.2 M cetyltrimethylammonium bromide (CTAB) was first prepared by stirring and heating on a hot plate until the CTAB fully dissolved, followed by cooling to 30 °C. Next, under continuous, vigorous stirring at 30 °C, 2.5 mL of filtered ultrapure water (VWR, Radnor, PA) and 2.5 mL of 1 mM $HAuCl_4$ were added into the CTAB solution. This was followed by the addition of 1 mL of freshly prepared 6 mM sodium borohydride. The solution was stirred for 2 min, during which the color changed from yellow to brown indicating the formation of small gold nanoparticle seeds of approximately 3-4 nm. The seed suspension was left to age for 30 min.

The growth solution was prepared by mixing 180 mg of CTAB and 22 mg of 5-bromosalicylic acid (Tokyo Chemistry Industry America, Portland, OR) in 5 mL of filtered ultrapure water which was heated and stirred until fully dissolved. This solution was cooled to 30 °C, after which 240 µL of 4 mM silver nitrate was added to the growth solution, quickly mixed, and then left undisturbed for 15 min at 30 °C. Next, 5 mL of 1 mM $HAuCl_4$ was added and the solution was stirred with a magnetic stir bar at 800 RPM for 15 min. 40 µL of 64 mM ascorbic acid was then vigorously stirred into the solution for 30 s until it became colorless, indicating the reduction of Au(III) to Au(I).

Finally, 4 μL of the aged gold seed suspension was added and stirred for another 30 s. The final suspension was then left to sit undisturbed for at least 12 h, after which the suspension was divided into 2 mL aliquots and centrifuged for 15 min at 8600 RCF and 30 °C. The supernatant was then discarded and each pellet of GNRs was resuspended in 2 mL of filtered ultrapure water. This centrifugation was repeated, and after discarding the supernatant, the final pellets were combined and resuspended to a total volume of 333 μL in filtered ultrapure water for 30-fold concentration.

3.2.2. Demonstration of gold nanorod etching for multicolor signal generation

The GNR etching precursor suspension for one reaction was made by mixing 8.25 μL of a solution containing 0.1 M CTAB and 0.1 M Tween 20 with 6.75 μL of synthesized GNRs, 22.5 μL of 1.4 M NaBr in 0.2 M citrate buffer (pH 4), and 7.5 μL of 100 μM horseradish peroxidase (HRP) in 0.1 M phosphate buffer (pH 6) in a well of a 96-well plate. To perform the etching reaction, 40 μL of varying concentrations of hydrogen peroxide (H_2O_2) in 3 mM NaOH were mixed into each well containing the GNR etching precursor suspension. After 10 min, photographs were taken with a Nikon D3400 DSLR camera (Nikon, Tokyo, Japan) in a controlled lighting environment and the UV-Vis spectra were observed using a Synergy H1 Hybrid Multi-Mode reader (BioTek, Winooski, VT).

3.2.3. Synthesis of porous platinum-shell gold-core nanozymes (PtNs)

PtNs were synthesized using a protocol modified from Loynachan *et al*.[86] In a 20 mL scintillation vial, 200 μL of a 20% w/w polyvinylpyrrolidone (PVP, 10 kDa) solution was mixed with 10 mL of 0.35 mM 20 nm gold nanoparticles (GNs) (nanoComposix, San Diego, CA) and

allowed to incubate for 5 min at room temperature (22°C). 200 μL of a 100 mM platinum chloride solution and 400 μL of a 100 mg/mL L-ascorbic acid solution were then added simultaneously and immediately mixed. The solution was then allowed to react in a 65 °C oil bath under magnetic stirring at 1200 RPM for 1 h. During this reaction, the platinum ions would be reduced by the L-ascorbic acid and deposit onto the surface of the GNs resulting in the formation of a thick, porous platinum shell. The resulting suspension was cooled in a 25 °C water bath for 1 h. To purify the particles from excess reagents, the suspension was split into 1 mL aliquots. Each aliquot was centrifuged twice at 8600 RCF for 12 min at 4 °C. The supernatant was removed, and the pellets were resuspended in 1 mL of filtered ultrapure water in between the spins. The supernatant from the original aliquot was saved after both spins and centrifuged separately at the same settings to capture any remaining particles in the supernatant. After the original aliquot and the saved supernatants were each centrifuged twice, the pellets were combined and resuspended in 500 μL of filtered ultrapure water, effectively doubling the concentration of PtNs relative to the unpurified PtN batch.

3.2.4. Synthesis of platinum-coated gold nanozymes (PtGNs)

Platinum-coated gold nanozymes were synthesized using a protocol derived from Gao *et al*.[63] 4 mL of 40 nm citrate-capped gold nanoparticles (GNs) (Nanocomposix, San Diego, CA) and 1827 μL of filtered ultrapure water were preheated to 90°C in an oil bath under magnetic stirring for 20 min. After preheating, 173 μL of a 0.82 mM chloroplatinic acid hydrate solution and 2 mL of a 3.3 mM ascorbic acid solution were injected separately into the gold nanoparticle suspension using a syringe pump at rates of 0.6 and 1.2 mL/h, respectively. The reaction was allowed to proceed for 1 h after the injection was complete.

3.2.5. Preparation of anti-transferrin (Tf) antibody-decorated porous platinum-shell gold-core nanozyme probes (anti-Tf PtNPs)

To create anti-Tf PtNPs, 41.5 µL of purified PtNs was first diluted in 458.5 µL of filtered ultrapure water. Next, 20 µL of a 0.1 M sodium borate (pH 9) solution was added to the PtN suspension. Subsequently, 2 µg of anti-Tf polyclonal antibody was added, and the mixture was placed on a microplate shaker at 700 RPM and allowed to react for 30 min at room temperature (22 °C) to allow the antibodies to adsorb and conjugate onto the surface of the PtNs through a combination of electrostatic interactions, hydrophobic interactions, and dative bonds. This was followed by the addition of 50 µL of a 10% w/v bovine serum albumin (BSA) solution in filtered ultrapure water in order to passivate the surface of the PtNs. After shaking at 700 RPM for 10 min, the suspension was purified to remove free antibodies using three centrifugation cycles at 8600 RCF and 4°C for 6 minutes each. The pellets resulting from the first two cycles were resuspended in 200 µL of 1% w/v BSA in filtered ultrapure water, while the pellet from the final centrifugation cycle was resuspended to a total volume of 25 µL in a 0.1 M sodium borate (pH 9) solution.

3.2.6. Preparation of anti-Tf antibody-decorated platinum-coated gold nanozyme probes (anti-Tf PtGNPs)

To create anti-Tf decorated platinum-coated gold nanozyme probes (anti-Tf PtGNPs), 20 µL of a 0.1 M sodium borate solution (pH 9) was first added to 500 µL of PtGNs. Then, 2 µg of primary anti-Tf antibody was added to the suspension and incubated on a microplate shaker at 700 RPM for 30 min at room temperature (22°C). 50 µL of a 10% (w/v) BSA in filtered ultrapure water solution was then added to the suspension and incubated at 700 RPM for 10 min. Free antibodies were removed with three centrifugation cycles at 8600 RCF and 4°C for 6 min each. For the first

two cycles, the pellet was resuspended in 200 μL of 1% (w/v) BSA in filtered ultrapure water, and the final pellet was resuspended to a final volume of 25 μL in a 0.1 M sodium borate (pH 6) solution.

3.2.7. Preparation of anti-digoxigenin antibody-decorated porous platinum-shell gold-core nanozyme probes (anti-digoxigenin PtNPs)

To create anti-digoxigenin PtNPs, 41.5 μL of purified PtNs were first diluted in 458.5 μL of filtered ultrapure water. Next, 2 μL of a 0.1 M sodium borate (pH 9) solution was added to adjust the PtN suspension pH to 7. Subsequently, 0.5 μg of anti-digoxigenin polyclonal antibody was added and the mixture was allowed to react for 30 min at room temperature (22 °C) to allow the antibodies to adsorb and conjugate onto the surface of the PtNs through a combination of electrostatic interactions, hydrophobic interactions, and dative bonds. This was followed by the addition of 50 μL of a 10% w/v bovine serum albumin (BSA) solution in filtered ultrapure water in order to passivate the surface of the PtNs. After reacting for 10 min, the suspension was purified of free antibodies using three centrifugation cycles at 8600 RCF and 4°C for 6 min each. The pellets resulting from the first two cycles were resuspended in 200 μL of 1% w/v BSA in filtered ultrapure water while the pellet from the final centrifugation cycle was resuspended to a total volume of 25 μL in a 0.06 M sodium borate (pH 9) solution.

3.2.8. Preparation of BSA-biotin-decorated gold nanoprobes (GNPs)

To create the BSA-biotin-decorated GNPs that bind to the control line, 2 μL of a 0.1 M sodium borate (pH 9) solution was first added to 500 μL of 40 nm GNs (nanoComposix, San Diego, CA) to achieve a pH of 7. Next, 8 μg of BSA-Biotin (Thermo Scientific, Waltham, MA)

was added to the suspension and incubated for 30 min at room temperature (22°C). Afterward, 50 µL of a 10% w/v BSA solution in filtered ultrapure water was added to the suspension and incubated for an additional 10 min. Free antibodies were then removed from the suspension using three centrifugation cycles at 8600 RCF and 4°C for 6 min each. The pellets resulting from the first two cycles were resuspended in 200 µL of 1% w/v BSA in filtered ultrapure water. The pellet from the final centrifugation cycle was resuspended to a total volume of 50 µL in a 0.07 M sodium borate (pH 9) solution.

3.2.9. Preparation of test strip for detection of transferrin

Proteins were printed and immobilized on the Unisart CN140 nitrocellulose membrane (Sartorius, Göttingen, Germany) using an Automated Lateral Flow Reagent Dispenser (Claremont BioSolutions LLC, Upland, CA) with the voltage setting at 4.5 V and a Fusion 200 syringe pump (Chemyx Inc, Stafford, TX) with a flow rate of 250 µL/min. The test line was formed by printing a solution of 2.5 mg/mL human transferrin in 25% w/w sucrose with two print cycles. The printed membrane was left in a vacuum-sealed desiccation chamber for 24 h.

To assemble the test strip, the nitrocellulose membrane was first adhered to an adhesive backing and cut into 5 mm wide strips. A 5 × 19 mm Standard 17 fiberglass paper (Cytiva, Marlborough, MA) sample pad was placed on the adhesive backing upstream of the test line and overlapping the nitrocellulose membrane by 2 mm. A 5 × 22 mm CF6 (Cytiva, Marlborough, MA) absorbent pad was placed on the adhesive backing downstream of the control line and overlapping the nitrocellulose membrane by 2 mm.

3.2.10. Preparation of test strip for detection of digoxin

Proteins were printed and immobilized on the Unisart CN95 nitrocellulose membrane (Sartorius, Göttingen, Germany) using an Automated Lateral Flow Reagent Dispenser (Claremont BioSolutions LLC, Upland, CA) with the voltage setting at 4.5 V and a Fusion 200 syringe pump (Chemyx Inc, Stafford, TX) with a flow rate of 250 μL/min. The test line was formed by printing a solution of 0.5 mg/mL digoxin-BSA (Fitzgerald Industries International, Acton, MA) in 25% w/w sucrose at two locations that were 1 mm apart with two print cycles each, such that the solution printed merged into one thick test line. The control line was formed by printing a solution of 1 mg/mL polystreptavidin (Biotez, Berlin, Germany) with two print cycles. The printed membrane was left in a vacuum-sealed desiccation chamber for 48 h.

To assemble the test strip, the nitrocellulose membrane was first adhered to an adhesive backing and cut into 5 mm wide strips. A 5 × 19 mm Standard 17 fiberglass paper (Cytiva, Marlborough, MA) sample pad was placed on the adhesive upstream of the test line and overlapping the nitrocellulose membrane by 2 mm. A 5 × 22 mm CF6 (Cytiva, Marlborough, MA) absorbent pad was placed on the adhesive backing downstream of the control line and overlapping the nitrocellulose membrane by 2 mm.

3.2.11. Design of the 3D printed holder

A holder was designed to orient the excised test lines in the incubation solution. This 3D printed device holds the test line tabs in place while the test lines are submerged in their respective wells. The 3D printed holder also utilizes a snapping mechanism to lock into the 96-well plate for consistent placement between trials. The three major components of the device are outlined in

Figure 3.1. The parts shown in gray were 3D printed using an Ultimaker 3 FDM 3D printer (Ultimaker B.V., Geldermalsen, Netherlands) out of Ultimaker CPE filament (co-polyester).

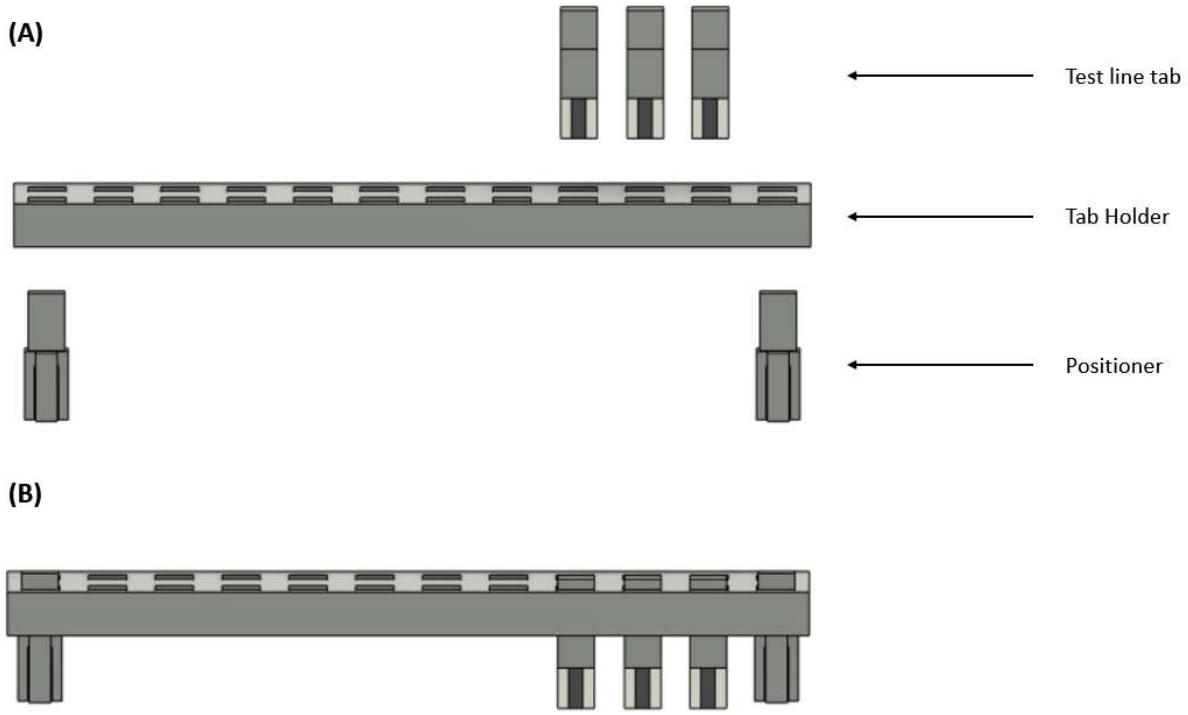

Figure 3.1. Design of the three main components of the 3D printed holder. (A) The deconstructed setup which consists of a test line tab that holds the excised test line, the tab holder which holds the test line steady in its respective well, and the positioner which snaps into the 96-well plate to hold the entire setup in place. (B) The fully assembled setup.

3.2.12. Oxidation of TMB using the LFA

60 µL of PBS was mixed with 3 µL of anti-Tf PtNPs or PtGNPs, 5 µL of running buffer (4% w/v 10 kDa polyvinylpyrrolidone, 0.4% w/v BSA, 0.4% w/v casein, and 0.4% w/v Tween 20 in 100 mM potassium phosphate buffer pH, 7.2), and 32 µL of Milli-Q water in a 2 mL tube. The sample pad of the LFA was then dipped into the 2 mL tube. After 7.5 min, an additional 50 µL of chase buffer (0.5% w/v 10 kDa polyvinylpyrrolidone, 0.05% w/v BSA, 0.05% w/v casein, and

0.05% w/v Tween 20 in 12.5 mM potassium phosphate buffer pH, 7.2) was added to the same tube. Following this antigen capture and detection step, a 5 mm x 5 mm portion of the test strip containing the test line was cut out and taped onto a 3D printed tab. The tab was then placed into a 3D printed holder above a 96-well plate. This holder positioned the tab in the center of the well with the test line region submerged in the TMB incubation solution (100 µL of 8.16 mM TMB and 10 mM H_2O_2 in 0.2 M citrate buffer (pH 4)) within the well. The 96-well plate with tab was placed on a microplate shaker at 600 RPM for 15 min. 50 µL of the TMB solution was then pipetted into 50 µL of a 3 M HCl stop solution and the visible absorbance at 450 nm was measured using a Synergy H1 Hybrid Multi-mode reader.

3.2.13. Quantitative detection of digoxin using the LFA with a multicolor readout

A 60 µL sample containing digoxin spiked into pooled human serum (Innovative Research Inc, Novi, MI) was mixed with 3 µL of anti-digoxigenin PtNPs, 4 µL of BSA-biotin-decorated GNPs, 5 µL of running buffer (4% w/v 10 kDa PVP, 0.4% w/v BSA, 0.4% w/v casein, and 0.4% w/v Tween 20 in 100 mM potassium phosphate buffer, pH 7.2), and 28 µL of Milli-Q water and placed in a 2 mL microcentrifuge tube. The sample pad of the LFA was then dipped into the 2 mL tube. After 7.5 min, an additional 50 µL of chase buffer (0.5% w/v 10 kDa PVP, 0.05% w/v BSA, 0.05% w/v casein, and 0.05% w/v Tween 20 in 12.5 mM potassium phosphate buffer, pH 7.2) was added to the same tube. The LFA was then run for an additional 5 min before photos were taken using a Nikon D3400 digital camera in a controlled lighting environment. Following this antigen capture and detection step, a 5 mm x 5 mm portion of the test strip containing the test line was cut out and taped onto a 3D printed tab. The tab was then placed into a 3D printed holder above a 96-well plate. This holder positioned the tab in the center of the well with the test line region

submerged in the H_2O_2 incubation solution (100 µL of 8 mM H_2O_2 in 3 mM NaOH) within the well. The 96-well plate with the tab was placed on a microplate shaker at 600 RPM for 25 min. 40 µL of the H_2O_2 incubation solution was then transferred into a separate 96-well plate containing the GNR etching precursor solution discussed previously in Section 2.2. After reacting for 10 min, photographs were taken with a Nikon D3400 DSLR digital camera in a controlled lighting environment and the UV-Vis spectra were measured using a Synergy H1 Hybrid Multi-mode reader.

3.3. Results and Discussion

3.3.1. Oxidation of TMB as a relative measure of nanozyme activity

When designing the combined workflow for our LFA step and multicolor output, the first decision we needed to make was whether to use PtNPs or PtGNPs. We wanted to use the particles which exhibited high catalytic activity to increase the sensitivity of the multicolor output to any small differences in test line intensity.

To compare the catalytic activity of the two particles, we made use of the peroxidase-like activity the particles exhibit when introduced into an acidic environment. We used this activity to oxidize TMB and measured the resulting absorbance values to compare the activity of the two nanozyme conjugates. The results of the two LFAs are shown in **Figure 3.2A** after the assay was run for 12.5 min. Both LFAs were run using negative samples on membranes designed to detect human transferrin via the competitive setup and therefore the dark test lines are expected.

The resulting oxidized TMB (before and after acid) along with the absorbance values at 450 nm are shown in **Figure 3.2B** and **Figure 3.2C** respectively. There is a significant increase in the oxidation of TMB when using PtNPs as compared to PtGNPs, which indicated a greater overall

catalytic activity of the PtNPs. Therefore, when designing our workflow, we used PtNPs to integrate the conventional LFA detection step with anisotropic GNR etching to achieve a semi-quantitative, multicolor output.

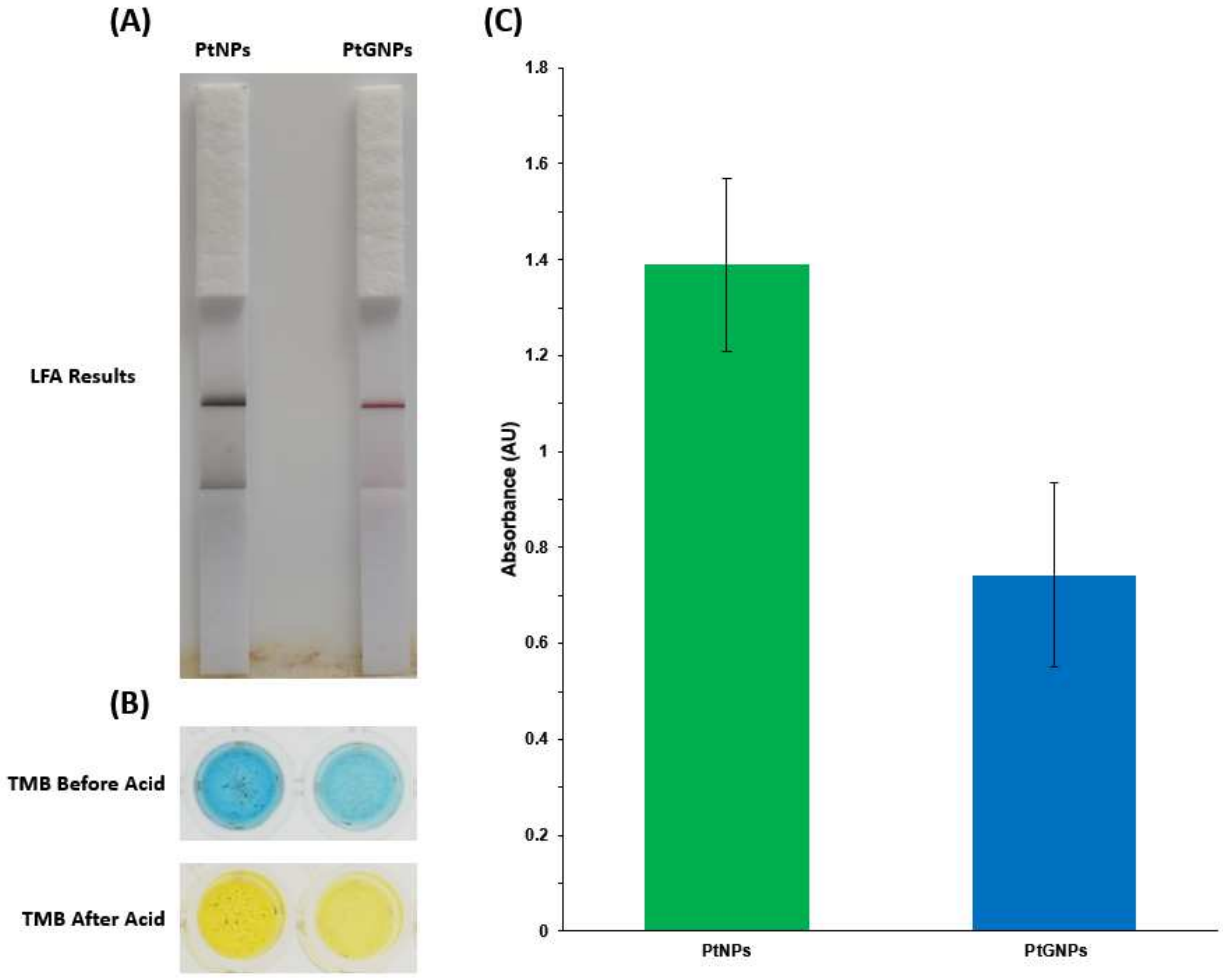

Figure 3.2. Comparison of Particle Activity. (A) LFA test lines resulting from tests run with PtNPs and PtGNPs. (B) Resulting intensity due to the oxidation of TMB both before and after the addition of the stop solution. (C) Resulting absorbance values measured at a wavelength of 450 nm. Data is presented as mean ± SD (n = 3).

3.3.2. Mechanism of the proposed LFA with a quantitative, multicolor readout

In this work, we propose that the LFA could be combined with platinum-shelled nanozymes possessing catalase-like activity and the anisotropic etching of GNRs to produce a

multicolor readout that is dependent on the concentration of the target analyte digoxin in a human serum sample. This would allow for naked-eye biomarker quantification without the need for electronic readers or complex and expensive laboratory equipment. The general assay procedure and mechanism are detailed in **Figure 3.3**. The serum sample is first mixed with the anti-digoxigenin PtNPs. The anti-digoxigenin antibodies conjugated onto the surface of the nanozymes are specific to digoxigenin and digoxin. Therefore, the anti-digoxigenin PtNPs capture any digoxin in the serum sample. Increasing concentrations of digoxin in the serum result in increased capture and thus greater saturation of the antibodies on the nanozyme surface.

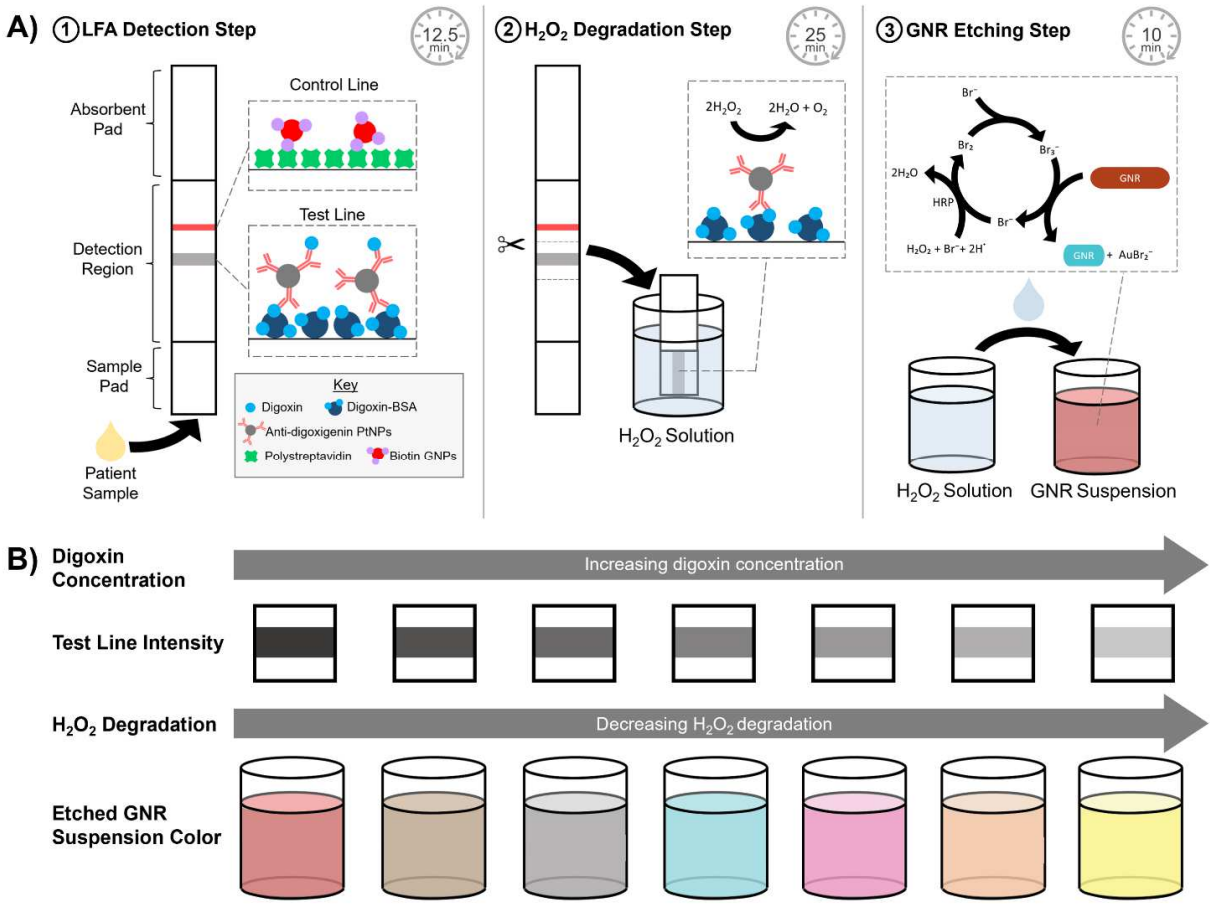

Figure 3.3. Simplified schematic of assay steps and resulting color output. (A) (1) Serum sample, control line GNPs, and test line PtNPs are applied to the LFA test strip and antigen capture

occurs in the detection zone. (2) After detection, the test line is excised and transferred to a basic H_2O_2 solution where the PtNPs bound to the test line catalyze the catalase-like degradation of H_2O_2. (3) After degradation, the H_2O_2 solution is transferred to a GNR suspension where any remaining H_2O_2 oxidizes bromide to form tribromide which leads to anisotropic etching of the GNRs. (B) The relationship between digoxin concentration, test line intensity, H_2O_2 degradation, and the etched GNR suspension color resulting in a semi-quantitative, multicolor readout.

After the sample is applied to the LFA test strip, it flows from the sample pad to the test line and finally into the absorbent pad. Because digoxin is a small molecule with very few unique binding epitopes, a competitive assay LFA format was utilized. As the sample flows past the test line composed of immobilized digoxin-BSA, the anti-digoxigenin antibodies on the PtNPs which are not saturated with digoxin from the serum sample will be able to bind to the test line. Thus, a low concentration of digoxin in the serum results in high binding of PtNPs to the test line, while a high concentration of digoxin results in low binding of PtNPs to the test line.

A 5 mm x 5 mm section of the LFA containing the test line is then cut out and transferred into a holder above a 96-well plate, where the test line is submerged in a hydrogen peroxide incubation solution. It has previously been demonstrated that noble metal nanoparticles—such as those composed of gold, silver, platinum, and palladium—possess pH-switchable catalytic activities.[24] In acidic conditions, they possess peroxidase-like activities where they catalyze the breakdown of hydrogen peroxide into free radicals which can oxidize chromogenic substrates.[25] In basic conditions, the nanoparticles possess catalase-like activities, where they catalyze the degradation of hydrogen peroxide into water and oxygen.[26] Therefore, we chose to use a basic pH for the hydrogen peroxide incubation solution so that the breakdown of hydrogen peroxide into water and oxygen would be catalyzed by any PtNPs bound to the test line. After this incubation, the concentration of hydrogen peroxide remaining in the solution would be directly related to the initial digoxin concentration in the original serum sample. A low concentration of digoxin results

in a high amount of PtNPs bound to the test line, fast degradation of the hydrogen peroxide, and thus less hydrogen peroxide remaining. A high concentration of digoxin, on the other hand, results in a low amount of PtNPs bound to the test line, slow degradation of hydrogen peroxide, and thus more hydrogen peroxide remaining.

To convert the concentration of hydrogen peroxide remaining in the incubation solution to the final visible multicolor readout, an oxidative GNR etching reaction is utilized. The hydrogen peroxide solution is transferred into a separate suspension containing GNRs, HRP, CTAB, Tween 20, and NaBr in a citrate buffer. The HRP would catalyze the oxidation of bromide ions to diatomic bromine (Br_2), which in the presence of excess bromide would be converted to the reactive species tribromide. The tribromide ions then form complexes with CTA^+ micelles due to strong electrostatic interactions. It has been suggested that this interaction both stabilizes the reactive tribromide ion and facilitates the transport of the tribromide to the surface of the GNRs which are coated with a CTA^+ bilayer.[87] The tribromide will oxidize the gold atoms on the tips of the GNRs, resulting in the anisotropic etching and shortening of the gold nanorods. By adding different concentrations of hydrogen peroxide into the GNR etching reaction, the GNRs would be etched to varying degrees, producing different sized GNRs. It is widely known that the optical properties of GNR suspensions are highly dependent on the particle aspect ratio (length divided by width) due to localized surface plasmon resonance, allowing for the production of a wide range of different colored suspensions through anisotropic etching. Ultimately, differences in the initial concentration of digoxin in the serum sample would result in GNRs being etched to different degrees that produce distinct differences in the visible color of the suspension that are easily interpreted by the naked eye.

3.3.3. Demonstration of GNR etching for multicolor quantification of hydrogen peroxide

While the oxidative anisotropic etching of GNRs has previously been reported to produce a wide spectrum of visible colors, studies that specifically etch GNRs using hydrogen peroxide and HRP without TMB have reported limited ranges in color production.[88,89]

To determine the full range of colors that could be produced from the GNR etching reaction, the added hydrogen peroxide concentration was varied from 0 to 2 mM. After reacting for 10 min, a wide spectrum of colors was produced (**Figure 3.4A**). Our experiment demonstrated that at least 10 distinct colors could be produced which are easily distinguishable by the naked eye. The resulting UV-Vis spectra confirmed that the GNRs are being etched, indicated by the progressive blue-shift in the longitudinal plasmon band that corresponds to a decreasing GNR aspect ratio (**Figure 3.4B**). The change in the longitudinal plasmon band peak wavelength was linear as a function of H_2O_2 concentration until 0.875 mM of H_2O_2 (**Figure 3.4C**). The resulting suspensions at 0.875 and 1 mM are pink and their corresponding UV-Vis spectra no longer have the longitudinal plasmon band that is characteristic of a gold nanorod. It is at this point that the GNRs have become spherical gold nanoparticles and have begun to etch evenly from all sides until no nanoparticles are left in the suspension. The yellow color of the solution from etching with 1.25, 1.5, and 2 mM H_2O_2 can be attributed to the further oxidation of the GNR etching reaction product $AuBr_2^-$ into $AuBr_4^-$ once all GNRs and spherical particles are completely degraded.[37] It is worth noting that the GNR etching reaction is extremely reproducible as shown in **Figure 3.4C**, where most error bars are not visible due to being so small.

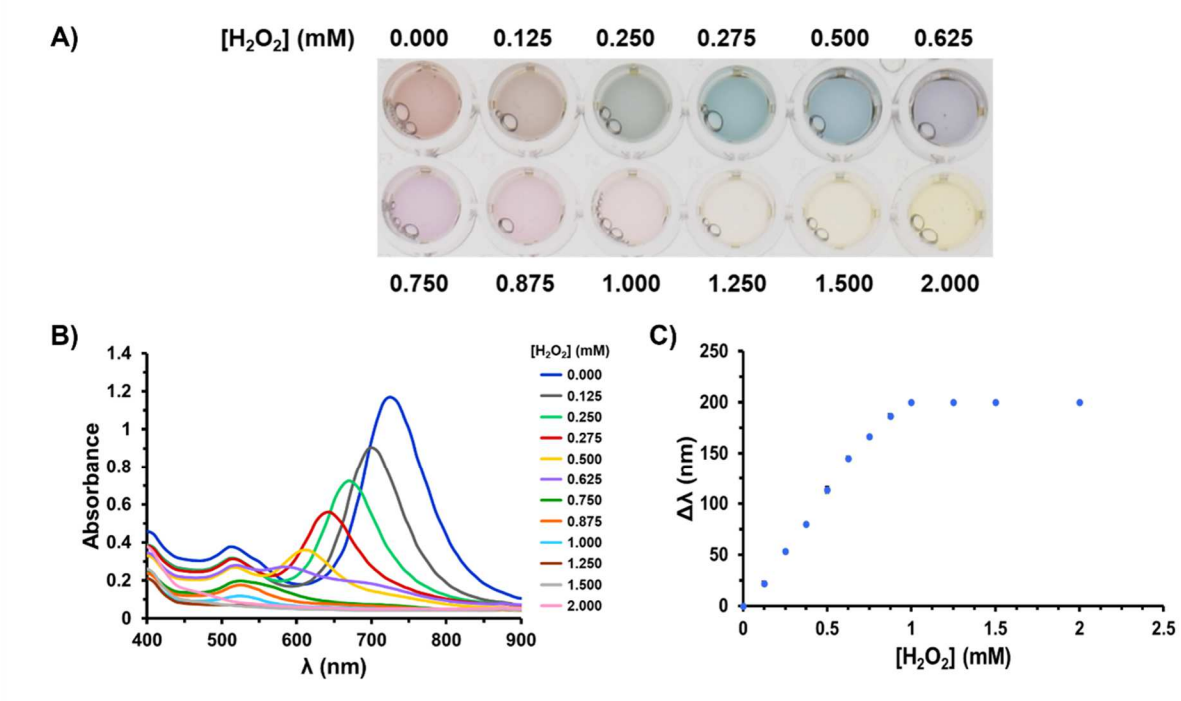

Figure 3.4. Etching results of GNRs exposed to varying H_2O_2 concentrations. (A) Photographs and (B) UV-Vis spectra resulting from exposing GNR etching suspensions to varying concentrations of H_2O_2. (C) Difference in the peak wavelength value of the longitudinal plasmon band after the GNR etching reaction relative to the condition without H_2O_2 for varying concentrations of H_2O_2. All data is presented in mean ± SD (n = 3).

3.3.4. Quantitative detection of digoxin using the LFA with a multicolor readout

We then moved on to evaluate whether our proposed assay could produce easily distinguishable colored results with small changes in digoxin concentration within the clinically relevant range of 0.5 to 3 ng/mL. The test lines produced after running the digoxin serum samples on the LFA for 12.5 min are shown in **Figure 3.5A**. As expected for a competitive assay format, the darkest test line is observed for the negative, and the test line intensity decreases as the concentration of digoxin increases. This indicates that there are differences in the amount of PtNPs bound to each test line for varying concentrations of digoxin, which is required for the hydrogen peroxide incubation step to leave different amounts of hydrogen peroxide to ultimately etch GNRs

to varying degrees. It is important to note it would be difficult for a user to reliably match the intensity of each line with a concentration of digoxin, especially the higher digoxin concentration range of 2-3 ng/mL where the test line intensity differences between each condition are minor.

The resulting GNR suspensions are shown in **Figure 3.5B**. It can be observed that the GNR etching reaction produced easily distinguishable colors that were dependent on the concentration of digoxin in the serum sample. This is in contrast to interpreting the test lines by intensity, where the visible differences can be slight and may be difficult to interpret quantitatively without the aid of an electronic reader. The color trend produced was also consistent with **Figure 3.4A**, and the UV-Vis results in **Figure 3.5C** and **Figure 3.5D** match the results from **Figure 3.4B** and **Figure 3.4C**, where decreasing digoxin concentrations result in a progressive blue-shift in the longitudinal plasmon band. This confirms that the increased amount of PtNPs bound to the test line with the lower digoxin concentrations degraded more of the hydrogen peroxide in the incubation solution when compared to the higher digoxin concentrations. Ultimately, our assay is able to quantitatively detect for digoxin in human serum by providing distinct colors below, within, and above the therapeutic window. Furthermore, not only can our assay be used to classify samples within these three categories, but it also provides more accurate measurements that have the potential to be used to calculate adjustments in dosage for individualized therapy.

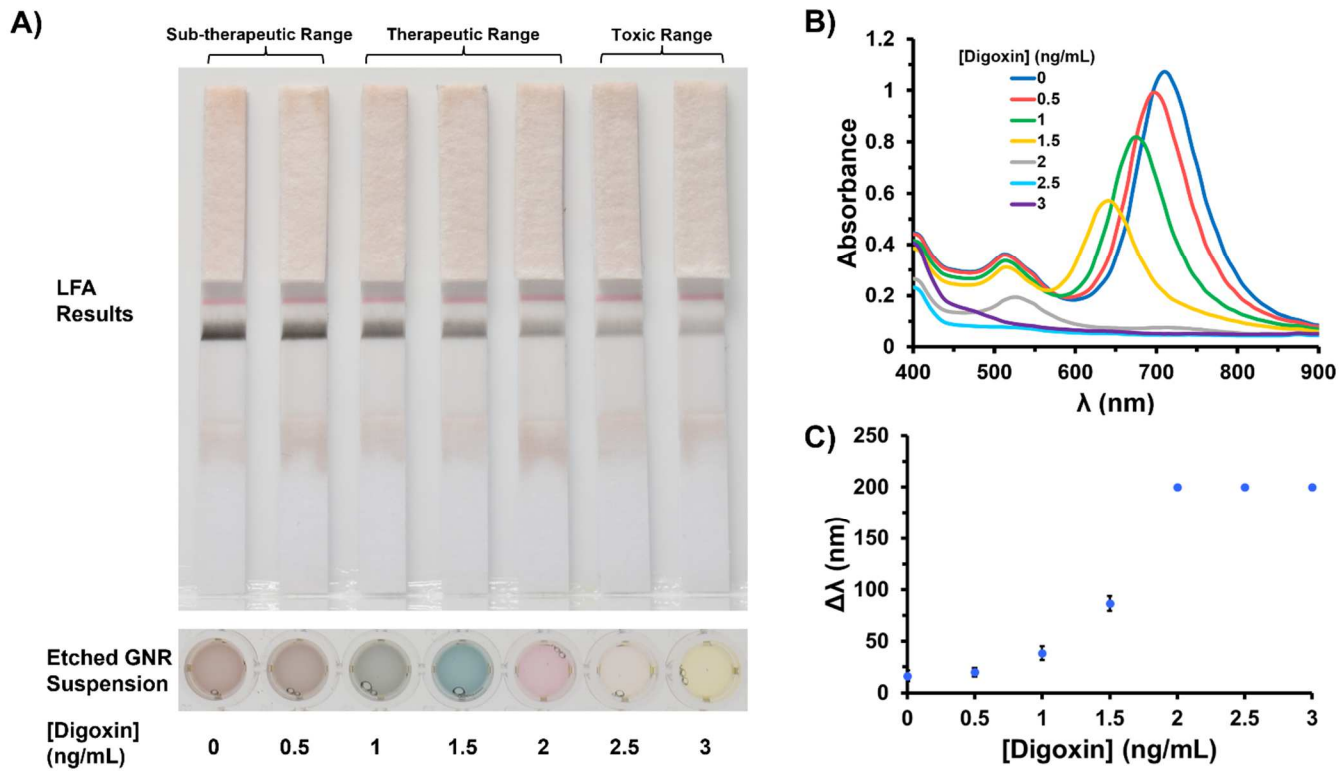

Figure 3.5. Multicolor output of the fully integrated assay. (A) LFA test lines and corresponding GNR suspensions resulting from the integrated LFA and GNR etching reaction. LFA test line intensity decreases and GNR etching increases with increase in digoxin concentration. Note that the control line is red instead of the gray color of the PtNPs as gold nanoparticles conjugated to BSA-biotin (GNPs) are binding to polystreptavidin on the control line. (B) UV-Vis spectra of the GNR suspensions. (C) Change in peak value of the UV-Vis longitudinal wavelength of the GNR suspensions relative to the value before the GNR etching reaction. Data is presented in mean ± SD (n = 3).

This technology could be useful in the quantitative detection of many other targets besides digoxin. Other therapeutic drug monitoring applications that our assay could be adapted to address include the quantitative monitoring of other therapeutic drugs such as levofloxacin for tuberculosis treatment, infliximab for inflammatory bowel diseases, antiepileptic drugs, and immunosuppressants to prevent organ rejection following transplant.[90] Besides therapeutic drug monitoring, we believe the multicolor, quantitative assay developed here could find applications in environmental contaminant testing.[91] We acknowledge that this technique in its current stage is

more complex than the conventional LFA because it requires additional handling steps, which could limit its use in an at home or in-field setting. However, it could serve to bridge the gap between the simple one step, qualitative LFA and the more complex quantitative, plasmonic ELISA. It is also the starting point for future work in the development of a fully paper-based version of this technology which will minimize user steps and eliminate the need for any laboratory equipment such as pipettes or microplate shakers.

3.4. Conclusions

In summary, we have developed a new method for the quantification of digoxin concentration in serum using the LFA combined with a gold nanorod etching reaction. To our knowledge, this is the first integration of the LFA with a gold nanorod etching reaction, as well as the first quantitative LFA with a multicolor readout that is dependent on the initial analyte concentration. We believe this work serves as a starting point for the development of a new generation of highly quantitative, lateral-flow assays which can be operated without the need for expensive laboratory equipment and electronic devices. Ultimately, this could lead to more effective patient management and treatment in resource-limited settings.

References

1 A. Boutayeb, *Handbook of Disease Burdens and Quality of Life Measures*, 2010, 531.

2 D. Mabey, R. W. Peeling, A. Ustianowski and M. D. Perkins, *Nat Rev Microbiol*, 2004, **2**, 231–240.

3 S. K. Vashist, *Biosensors (Basel)*, 2017, **7**, 62.

4 The top 10 causes of death, https://www.who.int/news-room/fact-sheets/detail/the-top-10-causes-of-death, (accessed April 26, 2022).

5 A. W. Martinez, S. T. Phillips, G. M. Whitesides and E. Carrilho, *Analytical Chemistry*, 2010, **82**, 3–10.

6 Y. Shen and G. Shen, *ACS Omega*, 2019, **4**, 5083–5087.

7 M. Tian, L. Lei, W. Xie, Q. Yang, C. M. Li and Y. Liu, *Sensors and Actuators B: Chemical*, 2019, **282**, 96–103.

8 W. Yang, X. bing Li, G. wen Liu, B. bing Zhang, Y. Zhang, T. Kong, J. jia Tang, D. na Li and Z. Wang, *Biosensors and Bioelectronics*, 2011, **26**, 3710–3713.

9 M. B. González-García and A. Costa-García, *Biosensors and Bioelectronics*, 2000, **15**, 663–670.

10 I. H. Cho, A. Bhunia and J. Irudayaraj, *International Journal of Food Microbiology*, 2015, **206**, 60–66.

11 H. Y. Yin, P. T. Chu, W. C. Tsai and H. W. Wen, *Food Chemistry*, 2016, **192**, 934–942.

12 W. Leung, C. P. Chan, T. H. Rainer, M. Ip, G. W. H. Cautherley and R. Renneberg, *Journal of Immunological Methods*, 2008, **336**, 30–36.

13 S. C. Lou, C. Patel, S. Ching and J. Gordon, *Clinical Chemistry*, 1993, **39**, 619–624.

14 D. W. Bradbury, A. E. Kita, K. Hirota, M. A. st. John and D. T. Kamei, *SLAS Technology*, 2020, **25**, 67–74.

15 E. Pilavaki and A. Demosthenous, *Sensors*, 2017, **17**, 2673.

16 R. Lal Makkar, S. Syeda Aliya, V. Borse and R. Srivastava, in *Optical Sensing and Detection V*, SPIE, 2018, vol. 10680, pp. 47–59.

17 L. M. Hu, K. Luo, J. Xia, G. M. Xu, C. H. Wu, J. J. Han, G. G. Zhang, M. Liu and W. H. Lai, *Biosensors and Bioelectronics*, 2017, **91**, 95–103.

18 Y. Chen, Q. Chen, M. Han, J. Liu, P. Zhao, L. He, Y. Zhang, Y. Niu, W. Yang and L. Zhang, *Biosensors and Bioelectronics*, 2016, **79**, 430–434.

19 M. You, M. Lin, Y. Gong, S. Wang, A. Li, L. Ji, H. Zhao, K. Ling, T. Wen, Y. Huang, D. Gao, Q. Ma, T. Wang, A. Ma, X. Li and F. Xu, *ACS Nano*, 2017, **11**, 6261–6270.

20 H. T. Kim, E. Jin and M. H. Lee, *Biosensors*, 2021, **11**, 191.

21 D. Serrate, J. M. de Teresa, C. Marquina, J. Marzo, D. Saurel, F. A. Cardoso, S. Cardoso, P. P. Freitas and M. R. Ibarra, *Biosensors and Bioelectronics*, 2012, **35**, 206–212.

22 B. Khlebtsov and N. Khlebtsov, *Nanomaterials*, 2020, **10**, 1–16.

23 P. D. Sinawang, V. Rai, R. E. Ionescu and R. S. Marks, *Biosensors and Bioelectronics*, 2016, **77**, 400–408.

24 J. Li, W. Liu, X. Wu and X. Gao, *Biomaterials*, 2015, **48**, 37–44.

25 Y. Liu, H. Wu, M. Li, J. J. Yin and Z. Nie, *Nanoscale*, 2014, **6**, 11904–11910.

26 Z. Zhu, Z. Guan, S. Jia, Z. Lei, S. Lin, H. Zhang, Y. Ma, Z. Q. Tian and C. J. Yang, *Angew Chem Int Ed Engl*, 2014, **53**, 12503–12507.

27 S. Singh, *Frontiers in Chemistry*, 2019, **7**, 46.

28 E. Petryayeva and U. J. Krull, *Analytica Chimica Acta*, 2011, **706**, 8–24.

29 J. Satija, N. Punjabi, D. Mishra and S. Mukherji, *RSC Advances*, 2016, **6**, 85440–85456.

30 N. T. Kim Thanh and Z. Rosenzweig, *Analytical Chemistry*, 2002, **74**, 1624–1628.

31 K. Sato, K. Hosokawa and M. Maeda, *J Am Chem Soc*, 2003, **125**, 8102–8103.

32 J. Satija, N. S. Punjabi, V. V. R. Sai and S. Mukherji, *Plasmonics*, 2014, **9**, 251–260.

33 E. Martinsson, M. M. Shahjamali, N. Large, N. Zaraee, Y. Zhou, G. C. Schatz, C. A. Mirkin and D. Aili, *Small*, 2016, **12**, 330–342.

34 J. Tharion, J. Satija and S. Mukherji, *Plasmonics*, 2015, **10**, 753–763.

35 A. Gole and C. J. Murphy, *Chemistry of Materials*, 2004, **16**, 3633–3640.

36 X. Ma, Y. Lin, L. Guo, B. Qiu, G. Chen, H. hao Yang and Z. Lin, *Biosens Bioelectron*, 2017, **87**, 122–128.

37 X. Ma, Z. Chen, P. Kannan, Z. Lin, B. Qiu and L. Guo, *Analytical Chemistry*, 2016, **88**, 3227–3234.

38 S. A. Alex, J. Satija, M. A. Khan, G. M. Bhalerao, S. Chakravarty, B. Kasilingam, A. Sivakumar, N. Chandrasekaran and A. Mukherjee, *Analytical Methods*, 2015, **7**, 5583–5592.

39 R. Zou, X. Guo, J. Yang, D. Li, F. Peng, L. Zhang, H. Wang and H. Yu, *CrystEngComm*, 2009, **11**, 2797–2803.

40 J. Cao, T. Sun and K. T. V. Grattan, *Sensors and Actuators B: Chemical*, 2014, **195**, 332–351.

41 P. Pokhrel, C. Hu and H. Mao, *ACS Sens*, 2020, **5**, 2283-2296.

42 D. Wu, T. Wu, Q. Liu and Z. Yang, *International Journal of Infectious Diseases*, 2020, **94**, 44–48.

43 Z. Bai, Y. Cao, W. Liu and J. Li, *Viruses 2021, Vol. 13, Page 1115*, 2021, **13**, 1115.

44 S. Kammila, D. Das, P. K. Bhatnagar, H. H. Sunwoo, G. Zayas-Zamora, M. King and M. R. Suresh, *Journal of Virological Methods*, 2008, **152**, 77–84.

45 X.-Y. Che, W. Hao, Y. Wang, B. Di, K. Yin, Y.-C. Xu, C.-S. Feng, Z.-Y. Wan, V. C. C. Cheng and K.-Y. Yuen, *Emerging Infectious Diseases*, 2004, **10**, 1947-1949.

46 D. Shan, J. M. Johnson, S. C. Fernandes, H. Suib, S. Hwang, D. Wuelfing, M. Mendes, M. Holdridge, E. M. Burke, K. Beauregard, Y. Zhang, M. Cleary, S. Xu, X. Yao, P. P. Patel, T. Plavina, D. H. Wilson, L. Chang, K. M. Kaiser, J. Nattermann, S. v. Schmidt, E. Latz, K. Hrusovsky, D. Mattoon and A. J. Ball, *Nature Communications*, 2021, **12**, 1931.

47 T. Li, L. Wang, H. Wang, X. Li, S. Zhang, Y. Xu and W. Wei, *Frontiers in Cellular and Infection Microbiology*, 2020, **10**, 470.

48 V. M. Corman, V. C. Haage, T. Bleicker, M. L. Schmidt, B. Mühlemann, M. Zuchowski, W. K. Jo, P. Tscheak, E. Möncke-Buchner, M. A. Müller, A. Krumbholz, J. F. Drexler and C. Drosten, *The Lancet Microbe*, 2021, **2**, e311–e319.

49 M. Linares, R. Perez-Tanoira, A. Carrero, J. Romanyk, F. Perez-Garcia, P. Comez-Herruz, T. Arroyo and J. Cuadros, *Journal of Clinical Virology*.

50 I. Santiago, *ChemBioChem*, 2020, **21**, 2880–2889.

51 In Vitro Diagnostics EUAs - Antigen Diagnostic Tests for SARS-CoV-2, https://www.fda.gov/medical-devices/coronavirus-disease-2019-covid-19-emergency-use-authorizations-medical-devices/in-vitro-diagnostics-euas-antigen-diagnostic-tests-sars-cov-2, (accessed July 9, 2021).

52 G. Lippi, A.-M. Simundic and M. Plebani, *Clinical Chemistry and Laboratory Medicine (CCLM)*, 2020, **58**, 1070-1076.

53 D. Basso, A. Aita, F. Navaglia, E. Franchin, P. Fioretto, S. Moz, D. Bozzato, C.-F. Zambon, B. Martin, C. Dal Prà, A. Crisanti and M. Plebani, *Clinical Chemistry and Laboratory Medicine (CCLM)*, 2020, **58**, 1579-1586.

54 J. Li and P. B. Lillehoj, *ACS Sensors*, 2021, **6**, 1270–1278.

55 D. Liu, C. Ju, C. Han, R. Shi, X. Chen, D. Duan, J. Yan and X. Yan, *Biosensors and Bioelectronics*, 2021, **173**, 112817.

56 D. W. Bradbury, M. Azimi, A. J. Diaz, A. A. Pan, C. H. Falktoft, B. M. Wu and D. T. Kamei, *Analytical Chemistry*, 2019, **91**, 12046–12054.

57 Q. Shen, H. Liang, J. Tian, C. Zhou, A. Gao, D. Wang, J. Ni and D. Cui, *Nano Biomedicine and Engineering*, 2020, **12**, 325–330.

58 J. Tian, K. Wang, Y. Liu, H. Liang, X. Li and D. Cui, *Nano Biomedicine and Engineering*, 2020, **12**, 306–310.

59 X. Liu, K. Wang, B. Cao, L. Shen, X. Ke, D. Cui, C. Zhong and W. Li, *Anal Chem*, 2021, **93**, 3626–3634.

60 J. Yang, K. Wang, H. Xu, W. Yan, Q. Jin and D. Cui, *Talanta*, 2019, **202**, 96–110.

61 X. Zhang, D. Li, C. Wang, X. Zhi, C. Zhang, K. Wang and D. Cui, *J Biomed Nanotechnol*, 2012, **8**, 372–379.

62 B. G. Andryukov, *AIMS Microbiology*, 2020, **6**, 280.

63 Z. Gao, H. Ye, D. Tang, J. Tao, S. Habibi, A. Minerick, D. Tang and X. Xia, *Nano Letters*, 2017, **17**, 5572-5579.

64 E. Jue, C. D. Yamanishi, R. Y. T. Chiu, B. M. Wu and D. T. Kamei, *Biotechnology and Bioengineering*, 2014, **111**, 2499-2507.

65 T. Peng, X. Liu, L. G. Adams, G. Agarwal, B. Akey, J. Cirillo, V. Deckert, S. Delfan, E. Fry, Z. Han, P. Hemmer, G. Kattawar, M. Kim, M. C. Lee, C. Lu, J. Mogford, R. Nessler, B. Neuman, X. Nie, J. Pan, J. Pryor, N. Rajil, Y. Shih, A. Sokolov, A. Svidzinsky, D. Wang, Z. Yi, A. Zheltikov and M. Scully, *Applied Physics Letters*, 2020, **117**, 2–5.

66 C. W. Tsao, A. W. Aday, Z. I. Almarzooq, A. Alonso, A. Z. Beaton, M. S. Bittencourt, A. K. Boehme, A. E. Buxton, A. P. Carson, Y. Commodore-Mensah, M. S. V. Elkind, K. R. Evenson, C. Eze-Nliam, J. F. Ferguson, G. Generoso, J. E. Ho, R. Kalani, S. S. Khan, B.

M. Kissela, K. L. Knutson, D. A. Levine, T. T. Lewis, J. Liu, M. S. Loop, J. Ma, M. E. Mussolino, S. D. Navaneethan, A. M. Perak, R. Poudel, M. Rezk-Hanna, G. A. Roth, E. B. Schroeder, S. H. Shah, E. L. Thacker, L. B. VanWagner, S. S. Virani, J. H. Voecks, N. Y. Wang, K. Yaffe and S. S. Martin, *Circulation*, 2022, **145**, e153–e639.

67 S. S. Virani, A. Alonso, E. J. Benjamin, M. S. Bittencourt, C. W. Callaway, A. P. Carson, A. M. Chamberlain, A. R. Chang, S. Cheng, F. N. Delling, L. Djousse, M. S. V. Elkind, J. F. Ferguson, M. Fornage, S. S. Khan, B. M. Kissela, K. L. Knutson, T. W. Kwan, D. T. Lackland, T. T. Lewis, J. H. Lichtman, C. T. Longenecker, M. S. Loop, P. L. Lutsey, S. S. Martin, K. Matsushita, A. E. Moran, M. E. Mussolino, A. M. Perak, W. D. Rosamond, G. A. Roth, U. K. A. Sampson, G. M. Satou, E. B. Schroeder, S. H. Shah, C. M. Shay, N. L. Spartano, A. Stokes, D. L. Tirschwell, L. B. VanWagner, C. W. Tsao, S. S. Wong and D. G. Heard, *Circulation*, 2020, **141**, E139–E596.

68 P. A. Heidenreich, J. G. Trogdon, O. A. Khavjou, J. Butler, K. Dracup, M. D. Ezekowitz, E. A. Finkelstein, Y. Hong, S. C. Johnston, A. Khera, D. M. Lloyd-Jones, S. A. Nelson, G. Nichol, D. Orenstein, P. W. F. Wilson and Y. J. Woo, *Circulation*, 2011, **123**, 933–944.

69 C. P. Mouton, M. Hayden and J. H. Southerland, *Prim Care*, 2017, **44**, e37–e71.

70 O. J. Ziff and D. Kotecha, *Trends in Cardiovascular Medicine*, 2016, **26**, 585–595.

71 G. Grześk, W. Stolarek, M. Kasprzak, M. Krzyżanowski, K. Szadujkis-Szadurska, M. Wiciński and E. Grześk, *Pharmacol Rep*, 2018, **70**, 184–189.

72 R. Valdes Jr, S. A. Jortani and M. Gheorghiade, *Clinical Chemistry*, 1998, **44**, 1096–1109.

73 J. S. Kang and M. H. Lee, *Korean J Intern Med*, 2009, **24**, 1–10.

74 K. Aonuma, T. Shiga, H. Atarashi, K. Doki, H. Echizen, N. Hagiwara, J. Hasegawa, H. Hayashi, K. Hirao, F. Ichida, T. Ikeda, Y. Maeda, N. Matsumoto, T. Sakaeda, W. Shimizu, M. Sugawara, K. Totsuka, Y. Tsuchishita, K. Ueno, E. Watanabe, M. Hashiguchi, S. Hirata, H. Kasai, Y. Matsumoto, A. Nogami, Y. Sekiguchi, T. Shinohara, A. Sugiyama, N. Sumitomo, A. Suzuki, N. Takahashi, E. Yukawa, M. Homma, M. Horie, H. Inoue, H. Ito, T. Miura, T. Ohe, K. Shinozaki and K. Tanaka, *Circ J*, 2017, **81**, 581–612.

75 B. Sanavio and S. Krol, *Front Bioeng Biotechnol*, 2015, **3**, 20.

76 J. Satija, N. Punjabi, D. Mishra and S. Mukherji, *RSC Advances*, 2016, **6**, 85440–85456.

77 L. Tang and J. Li, *ACS Sensors*, 2017, **2**, 857–875.

78 P. Yager, G. J. Domingo and J. Gerdes, *Annu Rev Biomed Eng*, 2008, **10**, 107–144.

79 W. Leung, C. P. Chan, T. H. Rainer, M. Ip, G. W. H. Cautherley and R. Renneberg, *J Immunol Methods*, 2008, **336**, 30–36.

80 H. Y. Yin, P. T. Chu, W. C. Tsai and H. W. Wen, *Food Chem*, 2016, **192**, 934–942.

81 A. E. Kita, D. W. Bradbury, Z. D. Taylor, D. T. Kamei and M. A. st. John, *Otolaryngol Head Neck Surg*, 2018, **159**, 824–829.

82 O. Mudanyali, S. Dimitrov, U. Sikora, S. Padmanabhan, I. Navruz and A. Ozcan, *Lab Chip*, 2012, **12**, 2678–2686.

83 J. Zhang, Z. Shen, Y. Xiang and Y. Lu, *ACS Sensors*, 2016, **1**, 1091–1096.

84 C. Ruppert, N. Phogat, S. Laufer, M. Kohl and H. P. Deigner, *Mikrochim Acta*, 2019, **186**, 119.

85 X. Ye, L. Jin, H. Caglayan, J. Chen, G. Xing, C. Zheng, V. Doan-Nguyen, Y. Kang, N. Engheta, C. R. Kagan and C. B. Murray, *ACS Nano*, 2012, **6**, 2804–2817.

86 C. N. Loynachan, M. R. Thomas, E. R. Gray, D. A. Richards, J. Kim, B. S. Miller, J. C. Brookes, S. Agarwal, V. Chudasama, R. A. McKendry and M. M. Stevens, *ACS Nano*, 2018, **12**, 279–288.

87 Q. Zhu, J. Wu, J. Zhao and W. Ni, *Langmuir*, 2015, **31**, 4072–4077.

88 L. Saa, M. Coronado-Puchau, V. Pavlov and L. M. Liz-Marzán, *Nanoscale*, 2014, **6**, 7405–7409.

89 L. Saa, R. Grinyte, A. Sánchez-Iglesias, L. M. Liz-Marzán and V. Pavlov, *ACS Applied Materials and Interfaces*, 2016, **8**, 11139–11146.

90 D. J. Touw, C. Neef, A. H. Thomson and A. A. Vinks, *Ther Drug Monit*, 2005, **27**, 10–17.

91 N. A. Meredith, C. Quinn, D. M. Cate, T. H. Reilly, J. Volckens and C. S. Henry, *Analyst*, 2016, **141**, 1874–1887.